Petrology of Birimian granitoids in southern Ghana - petrography and petrogenesis

Mikael Grenholm

Kandidatuppsats i Geologi vid Lunds Universitet, nr. 285
(15 hskp/ECTS)

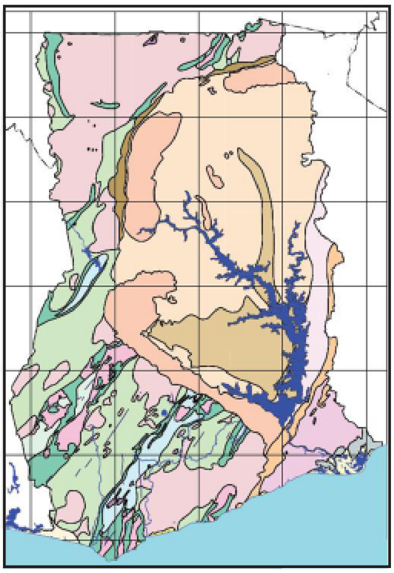

Department of Earth- and Ecosystem Sciences
Division of Geology
Lund University
2011

Petrology of Birimian granites in southern Ghana – petrography and petrogenesis

Bachelor thesis, 15hp

Mikael Grenholm

Supervisor: Anders Scherstén.

Department of Earth and Ecosystem Sciences
Division of Geology
Lund University

2011

Contents

1 Introduction **6**
2 Geological setting **7**
3 Geodynamic model **7**
4 Methods **10**
4.1 Fieldwork 10
4.2 Geochemistry 10
4.3 Light microscopy 10
4.4 Geochronology 11
5 Sample descriptions **11**
5.1 Belt granitoids 11
5.1.1 ASGH 004A, 004B, 004C, 004D 11
5.1.2 ASGH 007A 11
5.1.3 ASGH 019A 11
5.1.4 ASGH 032A, 032B 11
5.1.5 PK 102 12
5.1.6 PK 105 12
5.2 Basin granitoids 12
5.2.1 ASGH 001A 12
5.2.2 ASGH 003A, 003B, 003C 12
5.2.3 ASGH 022A, 022B, 022C, 022D, 022E 12
5.2.4 ASGH 025A, 025B 12
5.2.5 ASGH 028A, 028B 13
5.2.6 ASGH 030A 13
5.2.7 ASGH 034A 13
5.2.8 ASGH 039A 13
5.2.9 PK 101 13
5.2.10 PK 103 13
6 Results **13**
6.1 Geochemistry 13
6.1.1 Belt granitoids 14
6.1.1.1 ASGH 004B 14
6.1.1.2 ASGH 007A 14
6.1.1.3 ASGH 019A 14
6.1.1.4 ASGH 032A, 032B 15
6.1.1.5 PK 102 15
6.1.1.6 PK 105 15
6.1.2 Basin granitoids 15
6.1.2.1 ASGH 001A 15
6.1.2.2 ASGH 003A, 003B 16
6.1.2.3 ASGH 022A, 022D, 022E 16
6.1.2.4 ASGH 025A 16

Cover Picture: Geological map of Ghana. This map was compiled in 1994 by Watts, Griffit and McQuat Ltd., Lakewood, Colorado, USA (reference unknown).

6.1.2.5 ASGH 028A, 028B 16
6.1.2.6 ASGH 030A 17
6.1.2.7 ASGH 034A 17
6.1.2.8 ASGH 039A 17
6.1.2.9 PK 101 17
6.1.2.10 PK 103 17
7 Discussion 17
7.1 Petrogenesis of belt granitoids 17
7.1.1 Tectonic setting and source 17
7.1.2 Are belt granitoids TTGs? 20
7.1.2.1 First things first, what are TTGs? 20
7.1.2.2 So where do the belt granitoids fit in? 21
7.1.3 Spatial and temporal changes among the belt granitoids 23
7.2 Petrogenesis of basin granitoids 24
7.2.1 Tectonic setting 24
7.2.1.1 Leucocratic granites 24
7.2.1.2 Two-mica, biotite and biotite-hornblende granitoids 26
7.2.1.3 Winneba granitoid 29
7.3 Eburnean orogeny: metamorphism, alteration and deformation 29
8 Conclusions 30
9 Acknowledgements 30
10 References 31
Appendix A 34
Appendix B 36
Appendix C 37

Petrology of Birimian granitoids in southern Ghana - petrography and petrogenesis

MIKAEL GRENHOLM

Grenholm, M., 2005: Petrology of Birimian granitoids in southern Ghana - petrography and petrogenesis. *Bachelor thesis in geology, Lunds university,* Nr. , 38 pp. 15 points.

Abstract:
The Paleoproterozoic Birimian terrane consists of volcanic and sedimentary rocks occurring in greenstone belts and metasedimentary basins that have been intruded by two generations of granitoids. The Birimian terrane comprises a large part of the West African craton. It formed during a period of extensive juvenile magmatism that led to the creation of a large area of continental crust. Many questions remain unanswered regarding the tectonic setting in which this crust-forming event occurred. The two generations of granitoids—broadly divided into older belt and younger basin types - are an important key to understanding the geodynamic evolution of the Birimian terrane. The purpose of this thesis has been to determine in what tectonic setting granitoids - both belt and basin types - from the Birimian terrane in southern Ghana were emplaced in.

The belt type granitoids were emplaced in a subduction setting between 2232-2169 Ma. They share many similarities with TTGs such as being sodic and HREE-depleted indicating that they were derived from a slab melt. However, they also show variable interaction with the mantle as well as a calc-alkaline behavior. It would therefore appear that the granitoids originated as slab melts but were the angle of the subducting slab was steep enough to allow the melt to interact with the mantle wedge.

The basin granitoids formed through crustal anatexis in association with the Eburnean orogeny and have ages between 2134-2098 Ma. With the exception of the Winneba granitoid melting occurred in water-saturated conditions leading to preferential melting of plagioclase. Melting may have initiated in transcurrent deformation zones where water was supplied from dehydrating sediments. The Winneba granitoid formed through dehydration melting. This may explain why it is younger then adjacent basin granitoids given that dehydration melting occurs at higher temperatures then water-saturated melting.

During the Eburnean orogeny the Birimian terrane was subjected to greenschist facies metamorphism. Two granitoids from the Sefwi and Ashanti belt has been extensively altered by hydrothermal fluids, possibly in association with the formation of hydrothermal gold mineralizations.

Keywords: Ghana, Birimian, granitoids, subduction, TTG, water-saturated melting, transcurrent deformation

Mikael Grenholm, Department of Earth and Ecosystem Sciences, Division of Geology, Lunds Universitet, Sölvegatan 12, SE-223 62 Lund, Sweden. E-mail: mikael.grenholm@live.com

Petrologi på Birimiska granitoider i södra Ghana - petrografi och petrogenes

MIKAEL GRENHOLM

Grenholm, M., 2005: Petrologi på Birimiska granitoider i södra Ghana - petrografi och petrogenes. *Examensarbeten i geologi vid Lunds universitet*, Nr, 38 sid. 15 poäng.

Sammanfattning:
Den Paleoproterozoiska Birimiska terrinen består av vulkaniska och sedimentära bergarter i grönstensbälten och metasedimentära bassänger som har blivit intruderade av två generationer granitoider. Den Birimiska terrinen utgör en stor del av den västafrikanska kratonen. Den bildades under en period med omfattande juvenil magmatism som skapade stora volymer med kontinental jordskorpa. Många frågor angående den tektoniska miljön i vilken denna process ägde rum är fortfarande obesvarade. De två generationer av granitoider - grovt indelade i äldre bält- och ocu yngre bassäng-typer - utgör en viktig nyckel till förståelsen för den Birimiska terranens geodynamiska utveckling. Syftet med detta examensarbete var att bestämma i vilken tektonisk miljö granitoider - både bält- och bassäng-typer - från den Birimiska terranen i södra Ghana bildades.

Bält-granitoiderna bildades i en subduktions-miljö mellan 2232-2169 Ma. De har många likheter med TTGs såsom att dem är Na-rika och uppvisar låga HREE-värden vilket indikerar att de bildades genom smältning av en subducerande oceanskorpa. Dock uppvisar de också tecken på interaktion med mantel samt ett calc-alkalint beteende. De verkar därför som om granitoiderna bildats genom en slab-smälta men där subduktionsvinkeln på oceanskorpan var tillräckligt stor för att smältan skulle kunna reagera med mantel-kilen.

Bassäng-granitoiderna bildades genom krustal anatexis i samband med den Eburniska orogenesen och har åldrar mellan 2134-2098 Ma. Undantaget Winneba-graniten så skedde smältningen i vatten-mättade förhållanden vilket ledde till preferentiel smältning av plagioklas. Smältning kan ha skett i diagonal-förkastningar där vatten har tillförts från dehydrerande sediment. Winneba-graniten bildades genom dehydreringssmältning. Detta kan förklara varför den är yngreän närliggande bassäng-granitoider då dehydrerings-smältning äger rum vid högre temperaturer än vatten-mättad smältning.

Metamorfos i Birimiska terrinen under den Eburniska orogensen uppgick till grönskiffer-facies. Två granitoider från Sefwi- och Ashanti-bältena har blivit kraftigt omvandlade av hydrothermala fluider, möjligen i anslutning med bildandet av hydrotermala guld-mineraliseringar.

Nyckelord: Ghana, Birimian, granitoids, subduction, TTG, water-saturated melting, transcurrent deformation

Mikael Grenholm, Institutionen för Geo– och Ekosystemvetenskaper, Enheten för Geologi, Lunds Universitet, Sölvegatan 12, SE-223 62 Lund. E-post: mikael.grenholm@live.com

1 Introduction

A large portion of the West African craton is comprised of the Paleoproterozoic Birimian terrane. It constitutes a major crust-forming event in which greenstone belts and metasedimentary basins - intruded by several suites of granitoids - formed between 2.35-1.98 Ga through extensive juvenile magmatism (e.g. Abouchami *et al.* 1990; Leube *et al.* 1990; Boher *et al.* 1992; Taylor *et al.* 1992; Feybesse *et al.* 2006).

Abouchami *et al.* (1990) and Boher *et al.* (1992) showed that the majority of Birimian rocks had radiogenic ε_{Nd}-values and Sm-Nd model ages clustering around 2.3-2.4 Ga. The few values that were unradiogenic and had higher model ages, indicating an older crustal component, were found in the contact between Birimian and older Archean terranes (Abouchami *et al.* 1990; Leube *et al.* 1990; Taylor *et al.* 1992). The presence of pillow lavas, marine sediments and the lack of an older crustal component led Abouchami *et al.* (1990) and Boher *et al.* (1992) to infer that the Birimian terrane had been deposited in an intra-oceanic setting.

The Birimian terrane holds many similarities to Archean cratons, both in terms of its structure as well as its composition; juvenile magmatism (Abouchami *et al.* 1990; Boher *et al.* 1992), tonalite-trondhjemite-granodiorite (TTG)-style granitoids (e.g. Doumbia *et al.* 1998) and alternating greenstone belts and metasedimentary basins (Davis *et al.* 1994) are features encountered in many Archean terranes. This has led some authors to suggest that the Birimian terrane represents a transition between Archean and Proterozoic processes, perhaps due to an unevenly cooling earth in which parts of the mantle maintained a higher - “Archean” - geotherm into the Proterozoic (Sylvester & Attoh 1992; Doumbia *et al.* 1998).

Many aspects regarding the geodynamic evolution of the Birimian terrane remains unanswered. Some authors suggest that it originated as an oceanic plateau of flood basalts in association with plume activity (Abouchami *et al.* 1990; Boher *et al.* 1992). Others propose that it instead has formed through accretion of island arcs (Sylvester & Attoh 1992; Hirdes *et al.* 1996; Hirdes & Davis 2002). However, it is possible that both processes have contributed to the buildup of various parts of the Birimian terrane (Hirdes *et al.* 1996).

The emplacement of granitoids plays a crucial part in the formation of continental crust. The greenstone belts and metasedimentary basins of the Birimian terrane have been intruded by several suites of granitoids of

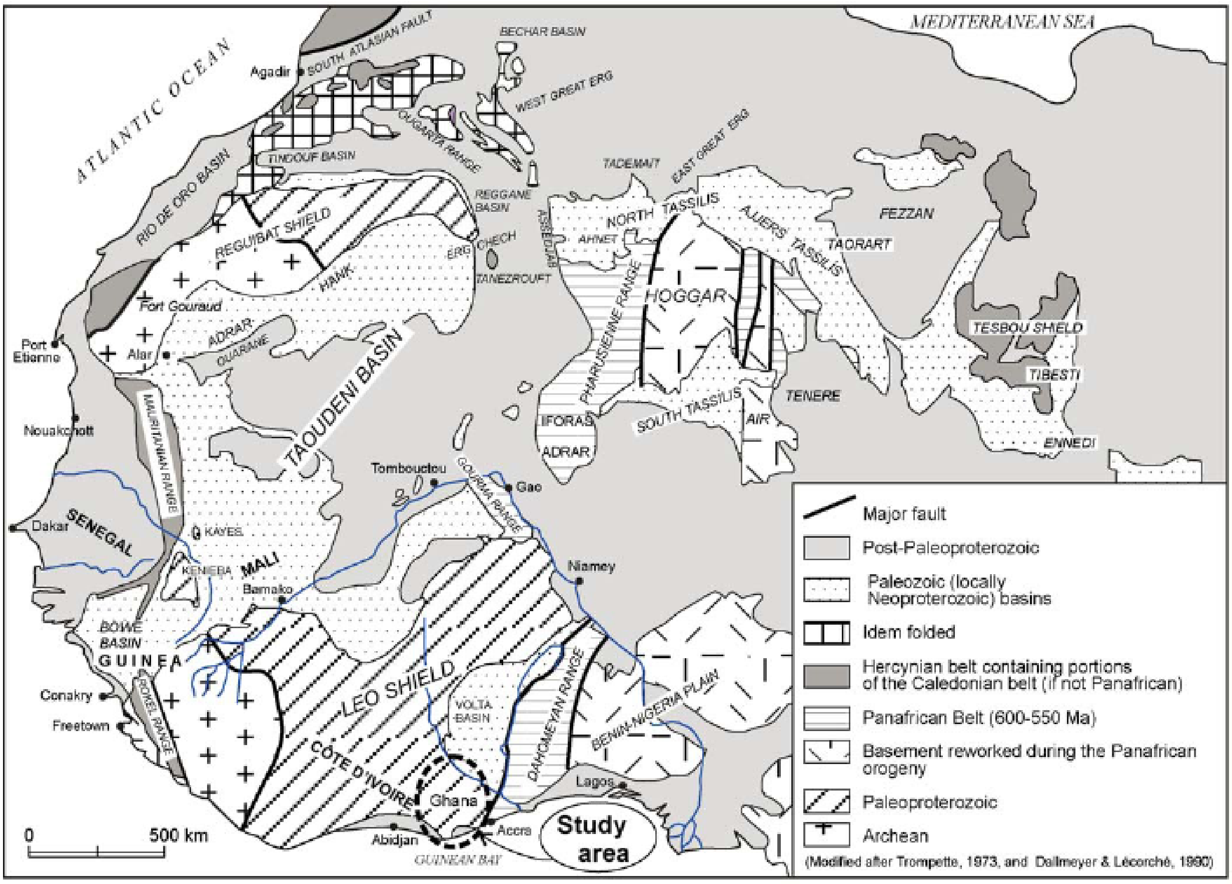

Fig. 1. Geological map over the West Africa craton. Study area is encircled (from Feybesse *et al.* 2006).

varying age and composition (e.g. Hirdes *et al.* 1992). These can be divided into two main types; the older I-type belt and the younger S-type basin granitoids (Leube *et al.* 1990; Hirdes *et al.* 1992). The belt types are either believed to be related to subduction processes (Boher *et al.* 1990; Hirdes *et al.* 2002) or to basal melting of a thick oceanic plateau (Doumbia *et al.* 1998). Basin type granitoids are believed to have formed through infra-crustal melting, either during crustal thickening or trans-current shearing (Leube *et al.* 1990; Doumbia *et al.* 1998; Feybesse *et al.* 2006; Lompo *et al.* 2010).

Determining through which processes the granitoids were emplaced is an important key to understanding the geodynamic evolution of the Birimian terrane. This thesis aims to determine the tectonix setting of granitoids from southern Ghana. The study is based on granitoids collected by Anders Schérsten.

2 Geological setting

The West African craton can be broadly divided into three domains (fig.1) (references in Abouchami *et al.* 1990 and Boher *et al.* 1992); the northern Reguibat shield, the southern Leo shield - both of which are Archean -Paleoproterozoic in age - and the central Neoproterozoic-Paleozoic Taoudeni basin which separates the two shields from each other. Pan-African (0.6 Ga) mobile belts mark the eastern limit of the craton. Both the Reguibat and Leo shield contain a W-SW Archean (~2.7 Ga) and an E-NE Birimian domain that are separated by a shear zone. It has been suggested that this is a common shear zone that extends under the Taoudeni basin. However, the Kedougou-Kenieba and Kayes inliers on the western edge of the West African Craton, halfway between the Reguibat and Man-Leo shields, consist of Birimian formations which do not show an Archean component. For this reason it is believed that the Taoudeni basin is underlain with a Birimian basement. Apart from the West African craton Birimian rocks are also present in south-central Sahara and the São Luis craton of northeastern Brazil. The Sao Luis craton is believed to have been attached to the southeastern corner of the Birimian terrane during the Paleoproterozoic (references in Abouchami *et al.* 1990, Boher *et al.* 1992 and Feybesse *et al.* 2006).

The Birimian domain in the Leo shield is called Baoulé Mossi and mainly covers Ghana, Ivory Coast, Burkina Faso, Guinea and southern Mali. Ghana is located in the southeastern corner of Baoulé Mossi.

The Birimian terrane in Ghana consists of greenstone belts separated by metasedimentary basins (fig. 2). These are NE-SW trending in southeastern Ghana but become increasingly more N-S trending towards the northwest. Together the greenstone belts and metasedimentary basins constitute the Birimian Supergroup. It is overlain with clastic sediment from the Tarkwaian group. Granitoids have intruded both the Birimian Supergroup and the Tarkwaian group (Leube *et al.* 1990; Taylor *et al.* 1992; Hirdes *et al.* 1992; Feybesse *et al.* 2006; de Kock *et al.* 2011)

The greenstone belts mainly consist of tholeiitic basalts and pillow lavas overlain by calc-alkaline andesites and dacites with interbedded volcaniclastic sediments (Leube *et al.* 1990; Sylvester & Attoh 1992).

The metasedimentary basins consists of felsic to intermediate volcaniclastics and metasedimentary rocks such as argillites, turbidites and chemical sediments (references in Abouchami *et al.* 1990; Leube *et al.* 1990).

The first generation of granitoids occurs mainly in greenstone belts but is also found in metasedimentary basins, particularly the Suhum and Cape Coast basins (Eisenlohr & Hirdes 1992; Feybesse *et al.* 2006). They are referred to as belt (also Dixcove) type granitoids (Leube *et al.* 1990). They occur as relatively small intrusives and many authors have noted that they have characteristics of TTG granitoids (e.g. Doumbia *et al.* 1998, de Kock *et al.* 2011).

The second generation of granitoids is found mainly in metasedimentary basins but also crosscut granitoids in greenstone belts. These are known as basin (or Cape Coast) type granitoids (Leube *et al.* 1990). They often occur as large batholiths within sedimentary basins in association with transcurrent faults and migmatites (Leube *et al.* 1990; Doumbia *et al.* 1998; Feybesse *et al.* 2006; Lompo 2010).

In addition to the belt and basin type granitoids, which are the two main types found in Ghana, there are the Winneba and Bongo granitoids. The Winneba type from the southern Kibi-Winneba belt is the only granitoid encountered in Ghana with an isotopic composition that indicates it was at least partly derived from Archean crust (Sm-Nd model age of 2.6 Ga). (Leube *et al.* 1990; Taylor *et al.* 1992). Paleocontinental reconstructions suggest that the São Luis Craton was connected to the southeastern West African craton during the Paleoproterozoic (references in Abouchami *et al.* 1990; Feybesse *et al.* 2006). The Bongo type is a K-rich and peraluminous granitoid (Leube *et al.* 1990; Eisenlohr & Hirdes 1992).

3 Geodynamic model

Feybesse *et al.* (2006) presented a geodynamic model for the Birimian terrane in southern Ghana. They divided its geological evolution into two cycles; the Pre-Eburnean (2.35-2.10 Ga) and Eburnean (2.13-1.98 Ga). The Pre-Eburnean was further subdivided into four stages and the Eburnean into two.

The first stage (2.35-2.30 Ga) of the Pre-Eburnean cycle consisted of volcano-plutonic activity

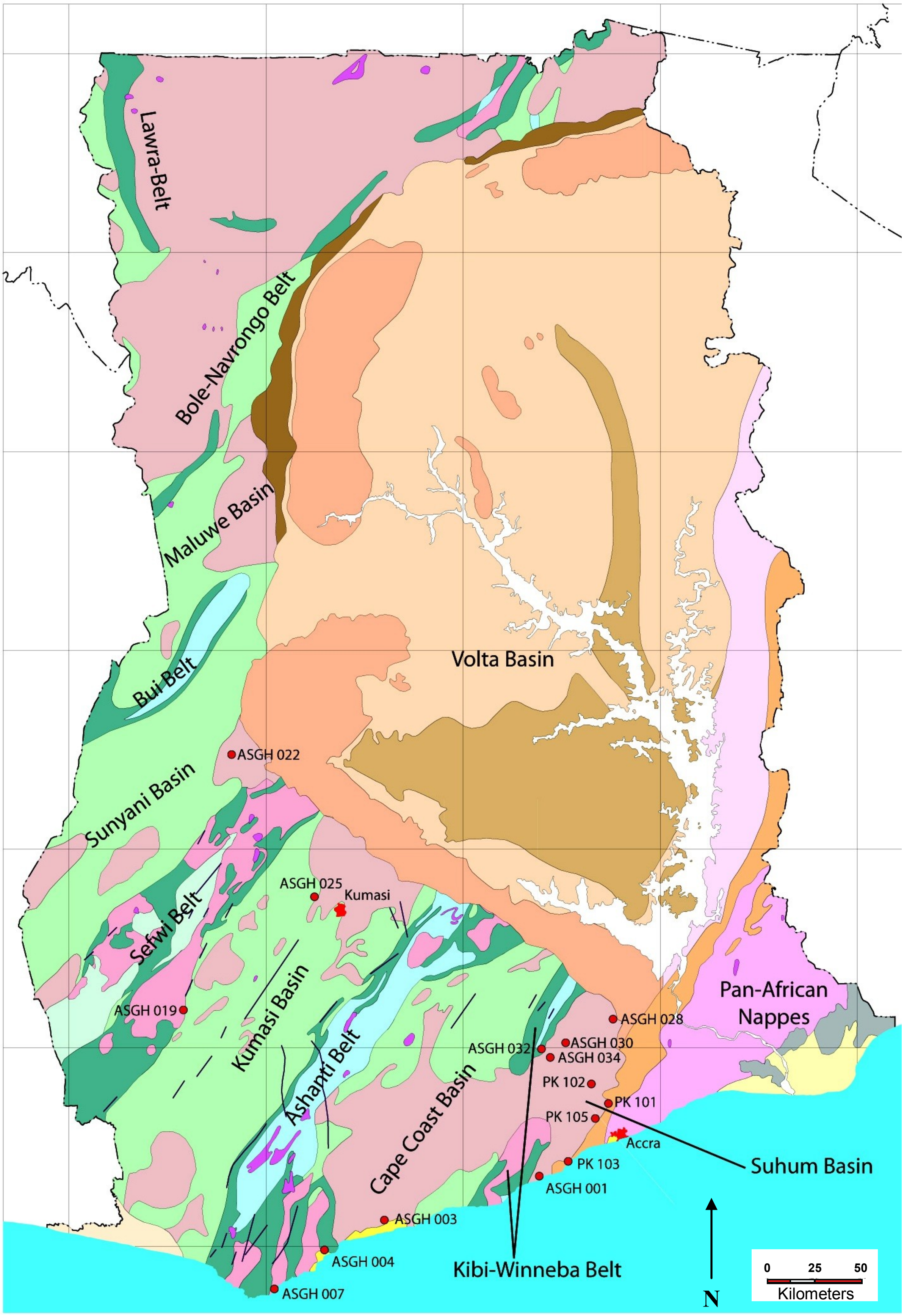
Lawra-Belt
Bole-Navrongo Belt
Maluwe Basin
Volta Basin
Bui Belt
ASGH 022
Sunyani Basin
ASGH 025
Kumasi
Sefwi Belt
ASGH 019
Kumasi Basin
Ashanti Belt
Cape Coast Basin
ASGH 028
ASGH 030
ASGH 032
ASGH 034
PK 102
PK 101
PK 105
Accra
PK 103
ASGH 001
ASGH 003
ASGH 004
ASGH 007
Pan-African
Nappes
Suhum Basin
Kibi-Winneba Belt
N
0 25 50
Kilometers

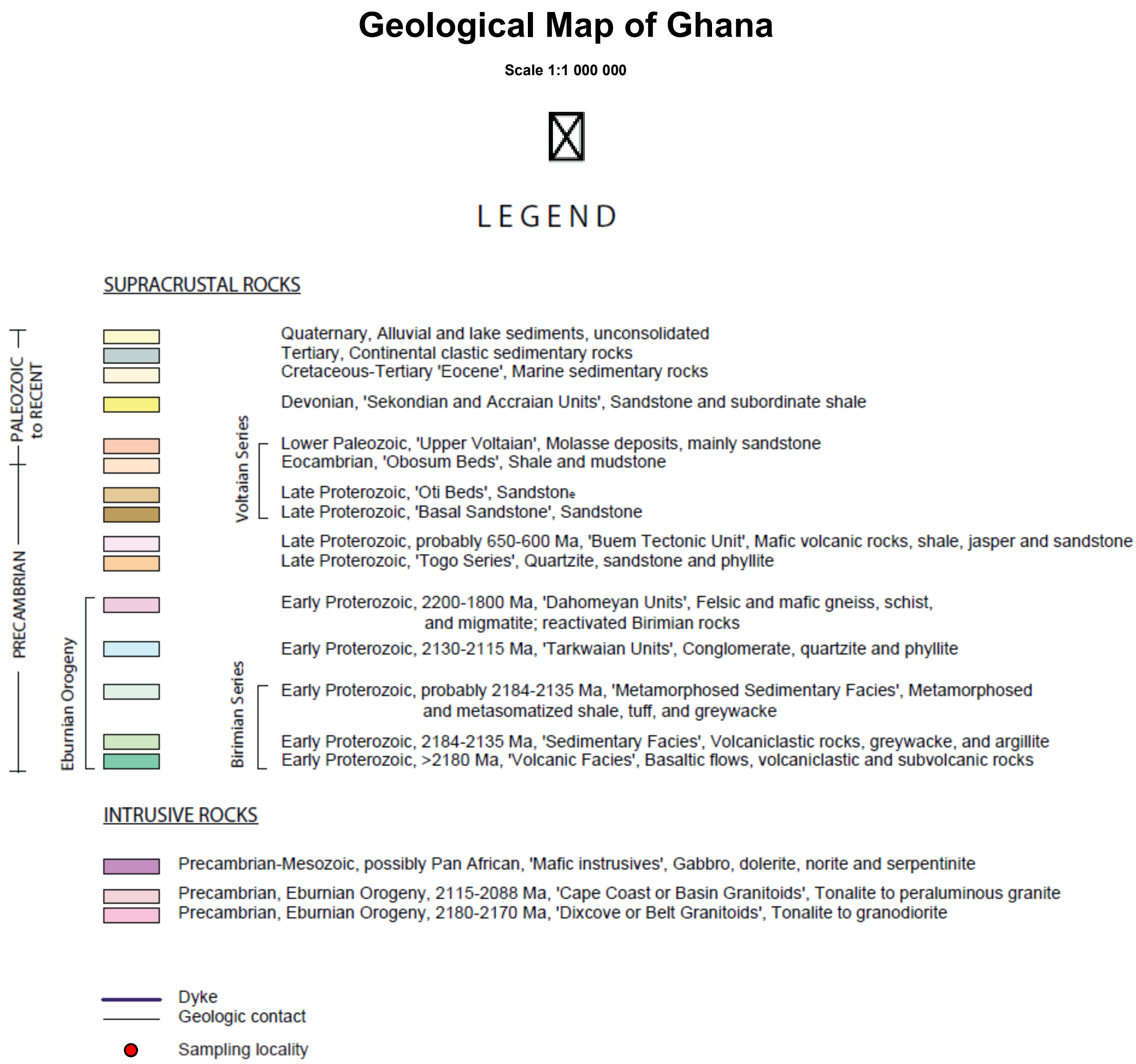

Fig. 2. A schematic geological map over Ghana. This map was compiled in 1994 by Watts, Griffit and McQuat Ltd., Lakewood, Colorado, USA (reference unknown).

and sedimentation along the margin of an Archean craton, probably the São Luis craton (Feybesse *et al.* 2006).

During the second stage (2.25-2.17 Ga) the protoliths of the greenstone belts - volcanic arcs or oceanic plateaus - were accreted to the São Luis craton (Feybesse *et al.* 2006). The greenstone belts were intruded by synvolcanic I-type granitoids (belt-type) (Eisenlohr & Hirdes 1992). Erosion of the greenstone belts formed coeval epiclastic sediments.

The third stage (2.16-2.15 Ga) consisted of emplacement of monzogranitic plutons into the greenstone belts. The monzogranites originated from basal, partial melting of the crust that was formed during the second stage. The emplacement of monzogranites marked the establishment of true continental crust (Feybesse *et al.* 2006).

Feybesse *et al.* (2006) considered the fourth stage (2.15-2.10 Ga) to be transitional between the Pre-Eburnean and Eburnean cycles. They argued that the newly formed crust at this stage was rifted, creating horst and graben structures. Erosional products derived from horsts were deposited in grabens forming sedimentary basins thus establishing the current belt and basin structure of the Birimian terrane. In this model the basement of the sedimentary basins is composed of the same rocks as the greenstone belts. Some authors have considered that the sedimentary basins formed contemporaneously with the greenstone belts (Leube *et al.* 1990), for example as foreland basins or accretionary prisms (Hirdes & Davis 2002). However, Feybesse *et al.* (2006)

based the assumption that rifting began at 2.15 Ga on the fact that sediment in the basins lays uncomformably on monzogranite formed during stage 3. Also, erosional products of monzogranite occur in the basins.

During the first stage (2.13-2.10 Ga) of the Eburnean cycle the Birimian terrane was affected by crustal shortening (D_1) in a NW-SE direction resulting in thrusting. Regional metamorphism during the Eburnean cycle was clockwise and reached amphibolite facies though it later retrogressed to greenschist facies (John *et al.* 1999).

Crustal shortening affected both the greenstone belts and sediments deposited in the basins. Minimum ages of detrital zircon from Tarkwaian sediment indicate that deposition was at least to some extent contemporaneous with the thrusting event. As such they are interpreted as late-orogenic molasse-type sediment. Deposition of sediments in basins during the fourth stage of the Pre-Eburnean cycle overlapped with crustal shortening during the first stage of the Eburnean orogeny. These sediments are therefore interpreted as flysch-type (Feybesse *et al.* 2006).

The final stage (2.095-1.980 Ga) of the Eburnean cycle marked a change in tectonic style from a compressional (D_1) to transcurrent regime ($D_{2\text{-}3}$) (Feybesse *et al.* 2006).

In the model of Feybesse *et al.* (2006) crustal anatexis and emplacement of synkinematic granitoids began in the first and continued during the second stage of the Eburnean Orogeny. Structures such as faults and shear zones formed during the second stage controlled the emplacement of syn-$D_{2\text{-}3}$ granitoids as well as the deposition of hydrothermal gold mineralizations. Intrusion of pegmatites and leucocratic granites occurred during the second stage (Feybesse *et al.* 2006).

The Bongo-type K-rich granitoids were emplaced during the late-first and second stage of the Eburnean. They are found in the Ashanti and Bole-Navrango belts where they intrude sediment from the Tarkwaian group (Eisenlohr & Hirdes 1992; Feybesse *et al.* 2006).

Magmatic activity ceased at ~2.05 Ga but the thermal effect of the Eburnean Orogeny lasted, based on K-Ar cooling ages of amphibolite, until 1.98 Ga (Feybesse *et al.* 2006; de Kock *et al.* 2011).

Hirdes *et al.* (1996) and Hirdes & Davis (2002) showed that magmatic activity, both in the greenstone belts and in the metasedimentary basins, were diachronous. The oldest ages among greenstone belts, belt granitoids and basin granitoids are found in Ghana with a trend of decreasing ages towards the Kedougou-Kenieba and Kayes inliers in the northwest.

Belt and basin granitoids in Ghana span intervals of 2232-2150 Ma and 2134-2088 Ma respectively (Hirdes & Davis 2002; This thesis). In Senegal belt granitoids are dated to 2082-2076 Ma. However, inherited zircons have ages up to 2155 Ma and detrital zircons have given ages up to 2165 Ma indicating the presence of older rocks. A basin granitoid in Senegal has been dated to 2079±2 Ma by Hirdes & Davis (2002).

The difference between the youngest age in Ghana and the basin granitoid in Senegal was interpreted by Hirdes and Davis (2002) to indicate that the Eburnean orogeny affected the Birimian terrane diacronously where the northwestern parts were affected by the orogeny at least 8 Ma after the southeastern parts.

4 Methods

4.1 Fieldwork

The granitoids presented in this thesis were collected from various localities in southern Ghana. The sample localities are displayed in fig. 2. ASGH samples were collected by Dr. Anders Schérsten during fieldwork in 2009 as a part of his VR-project. The PK samples were collected by Dr. Per Kalvig at the Denmark and Greenland Geological Survey (GEUS). Field observations used for the ASGH samples were based on field notes and photos provided by Anders Schérsten as well as personal communication. No field observations have been available for the PK samples. To simplify, the ASGH prefix will be omitted in the following text.

4.2 Geochemistry

Whole rock samples were hand-crushed and divided into suitable sizes for milling into whole rock powder using a wolfram-carbide swing mill. Whole rock powders were sent to ACME Analytical Laboratories Ltd. (www.acmelab.com, 2011-04-14) in Vancouver, Canada, to be analyzed for major and trace elements. Analyzes were made using ICP mass spectrometry and ICP emission spectrometry. Analyzes were performed on the following 21 samples: 001A, 003A, 003B, 004B, 007A, 019A, 022A, 022D, 022E, 025A, 028A, 028B, 030A, 032A, 032B, 034A, 039A, PK 101, PK 102, PK 103 and PK 105. The computer software GCDkit 2.3 (www.gcdkit.org/, 2011-08-17) by Janoušek *et al.* (2006) was used to plot the geochemical diagrams.

4.3 Light microscopy

Thin sections were prepared by Boguslaw Baginski in Warsaw and were studied using a polarizing light microscope at the Department of Earth- and Ecosystem Sciences at Lund University. Thin sections were prepared for all analyzed samples except 003B, 022A, 025A and 039A. Thin sections, for which there is no available chemical analyzes, were prepared and studied for the following samples; 003C, 004A, 004C, 004D, 022B, 022C and 025B. No point-counting was done and hence estimates of the relative abundance of quartz, K-feldspar and plagioclase were used in order to determine the granitoid composition of the samples.

4.4 Geochronology

Radiometric dating on 001A, 003A, 007A, 019A, 022A, 022C, PK 101, PK 102, PK 103 and PK 105 was performed by Dr. Anders Scherstén (personal communication). These ages are presented in Appendix C: table 1. A compilation of other published ages from the Birimian terrane in souhern Ghana are presented in Appendix C: table 2.

5 Sample descriptions

The analyzed samples are presented individually below with petrography and field observations. In cases were several samples were taken from the same locality they are presented together. Sampling localities are displayed in figure 2.

5.1 Belt Granitoids

5.1.1 ASGH 004A, 004B, 004C, 004D

The samples were collected from the southwestern Cape Coast basin. 004B is a biotite- and hornblende-bearing tonalite. 004A and 004C are leucocratic granites while 004D is an aplitic dyke. No age has been obtained for these samples. However, Oberthür *et al.* (1998) obtained an age of 2174±2 Ma (see Appendix C, table 2) from the same granitoid.

At the outcrop 004B is medium-coarse grained and has been intruded by 004A, 004C, 004D and a pegmatite. The pegmatite displays a pinch-and-swell structure meaning it is most likely pre-deformational. 004D is interpreted to post-date deformation as it cross-cut foliation in 004B.

All samples from the locality exhibit a foliation and dynamic recrystallization in the form of bulging grain boundaries and quartz subgrains. They also contain epidote-group minerals. In addition, 004A and 004D contains an alteration band with phrenite, muscovite and saussuritization.

5.1.2 ASGH 007A

007A is a biotite- and hornblende-bearing tonalite from the southern Ashanti belt. The sample has yielded an age of 2172±12 Ma (Anders Scherstén, unpublished data).

At the outcrop 007A is medium-coarse grained and isotropic, not showing any signs of deformation. Angular basaltic inclusions (<1 dm) are common.

The sample has a porphyritic texture with large euhedral plagioclase. It has been extensively altered through saussuritization and chloritization. It contains epidote-group minerals. Dynamic recrystallization is seen among quartz in the form of bulging grain boundaries and subgrains.

5.1.3 ASGH 019A

019A is a biotite- and hornblende-bearing tonalite from the Sefwi belt. It has been dated to 2169±13 Ma (Anders Scherstén, unpublished data).

The sample locality consisted of loose boulders. The boulders were medium grained and isotropic. No mafic inclusions were observed at the locality but are nonetheless believed to be present in the granitoid.

The sample is isotropic and has been extensively altered through saussuritization and chloritization. It contains epidote-group minerals. Dynamic recrystallization is seen among quartz as bulging grain boundaries and subgrains.

5.1.4 ASGH 032A, 032B

These samples were collected from the northern Kibi-Winneba belt. 032A is a biotite- and hornblende-bearing granodiorite whereas 032B is a biotite-rich granodiorite. No age has been obtained for these samples. However, Feybesse *et al.* (2006) obtained an age of 2200±4 Ma (see Appendix C, table 2) from a porphyritic granodiorite in the northern Kibi-Winneba belt, close to the sample locality of 032A and 032B.

At the outcrop 032A is quartz (<3 cm) and K-feldspar porphyritic but also contain biotite grains up to 5 mm. 032B is a sample from rounded mafic inclusions that are common in 032A (fig. 3).

The samples are isotropic but show dynamic recrystallization through bulging grain boundaries; particularly in quartz, which also display subgrains. Both samples contain epidote-group minerals.

5.1.5 PK 102

PK 102 is a biotite- and hornblende-bearing granodiorite from the Suhum basin. It has been dated to 2180±4 Ma (Anders Scherstén, unpublished data).

The sample is foliated and display dynamic recrystallization through nucleation, bulging grain boundaries; particularly in quartz which also display subgrains. It contains epidote-group minerals.

5.1.6 PK 105

PK 105 is a biotite- and hornblende-bearing granodiorite from the Suhum basin. It has been dated to 2232±5 Ma (Anders Scherstén, unpublished data) which is the oldest age obtained on a granitoid in Ghana.

The sample is foliated and display dynamic recrystallization through bulging grain boundaries; particularly in quartz which also display subgrains. It contains epidote-group minerals and metamorphic muscovite.

5.2 Basin Granitoids

5.2.1 ASGH 001A

The sample is a Winneba type biotite-bearing granite. It is located in the southernmost part of the Kibi-Winneba

Fig. 3. Mafic enclave (032B) occuring within 032A. Note the rounded edge of the inclusion. Photo by Anders Scherstén.

belt and has been dated to 2090±60 Ma (Anders Scherstén, unpublished data).

At the outcrop it has a porphyritic texture and contains K-feldspar megacrysts. 001A is crosscut by a ~1 m thick pegmatite as well as aplitic dykes.

In thin section it shows dynamic recrystallization in the form of bulging grain boundaries. Quartz also displays subgrains. It also contains epidote-group minerals and metamorphic muscovite

5.2.2 ASGH 003A, 003B, 003C

The come from the southern Cape Coast basin. 003A and 003B are two-mica (predominantly biotite) granodiorites whereas 003C biotite-bearing tonalite. 003A has been dated to 2124±6 Ma (Anders Scherstén, unpublished data).

The outcrop is heterogeneous, displaying several intrusion stages. 003A is very coarse grained whereas 003B is medium grained. 003C occur as medium grained mafic xenolith, possibly metasedimentary in origin.

In thin section 003C shows dynamic recrystallization in the form of bulging grain boundaries and subgrains in quartz. 003C contains epidote-group minerals and metamorphic muscovite.

5.2.3 ASGH 022A, 022B, 022C, 022D, 022E

These samples were all taken from a locality in the Sunyani basin. Radiometric dating has yielded an age of 2094±4 Ma for 022A and, for 022C, an age of 2092±4 Ma (Anders Scherstén, unpublished data).

022A is a biotite-hornblende granitoid while 022B and 022D are biotite-muscovite tonalites. 022E is a biotite-muscovite granodiorite. 022C is a biotite-muscovite tonalite.

The outcrop is very heterogeneous with intermingling felsic and mafic bands (022A, 022B, 022D, and 022E) (fig. 4). 022C is a late leucogranitic pegmatite. It also contains abundant mica schist xenoliths.

022B, 022D and 022E contain epidote-group minerals. Along with 022C, they also display dynamic recrystallization in the form of bulging grains boundaries and quartz subgrains. 022B contains medium grained poikiloblastic garnet. 022B, 022C and 022D are foliated. The distribution of biotite and muscovite in 022D and 022E is relatively even. Biotite is more abundant in 022B.

5.2.4 ASGH 025A, 025B

These samples were taken from the northwestern Kumasi basin. 025A is a two-mica granitoid while 025B is leucocratic granite. No age has been obtained for these samples. However, published ages for granitoids in the Kumasi basin span 2090-2136 Ma (see Appendix C, table 2).

At the sample locality the granitoid contained biotite and subordinate muscovite but it was not possible to determine the abundance of plagioclase and K-feldspar. The granite is homogenous and completely unreformed. It is coarse and uneven grained with feldspar-grains up to 1-1.5 cm. 025A has been intruded by 3 generations of late stage veins and dykes. 025B (see Appendix A) was sampled from a late stage leucocratic granite vein.

025B exhibits dynamic recrystallization in the form of bulging grains boundaries and quartz subgrains. It also has epidote-group minerals.

5.2.5 ASGH 028A, 028B

028A and 028B were taken from a locality in the northern Suhum basin. Both samples are biotite- and hornblende-bearing granites. No age has been obtained for this sample. An age of 2132±4 Ma has been obtained from granitoid gneiss in the central Suhum basin. On the geological map, this granitic gneiss is the same rock type as the locality at which 028A and 028B were collected.

Fig. 4. Loose boulder from the locality of 022A, 022B, 022D and 022E showing migmatitic texture with mafic and felsic bands. Photo by Anders Scherstén.

The outcrop at the sample locality is complex (fig. 5). It is migmatitic with a mafic residue and granitic veins, both of which have been heavily folded. 028A is sampled from the granite which, at the locality, was K-feldspar porphyritic with ~1 cm large grains. It also displayed well developed epidote. 028B is taken from the residue.

In thin section the samples display dynamic recrystallization in the form of bulging grains boundaries and quartz subgrains. They also have epidote-group minerals.

5.2.6 ASGH 030A

030A is a biotite- and hornblende-bearing granite from the northern Kibi-Winneba belt. No age has been obtained from this sample. No ages for basin granitoids in the northern Kibi-Winneba belt are available. 001A, from the southern part of the belt, has an age of 2090±60 Ma (Anders Scherstén, unpublished data).

Fig. 5. The outcrop at the locality of 028A and 028B showing intermingling felsic (028A) and mafic (028B) domains. Photo by Anders Scherstén.

At the outcrop 030A was coarse grained and contained K-feldspar ~1-2 cm large K-feldspar phenocrysts Muscovite has been reported from the locality but was not found during field work. 030A also contained a large mica schist xenolith.

In thin section the samples display dynamic recrystallization in the form of bulging grains boundaries, nucleation and quartz subgrains. It also has epidote-group minerals.

5.2.7 ASGH 034A

034A is a foliated biotite- and hornblende-bearing granite from the northern Kibi-Winneba belt. No age has been obtained from this sample. No ages for basin granitoids in the northern Kibi-Winneba belt are available. 001A, from the southern part of the belt, has an age of 2090±60 Ma (Anders Scherstén, unpublished data).

At the outcrop 034A is coarse grained. It contains mica schist xenoliths and is cross-cut by pegmatites and microgranite dykes.

In thin section the samples display dynamic recrystallization in the form of bulging grains boundaries, nucleation and quartz subgrains. They also have epidote-group minerals.

5.2.8 ASGH 039A

039A is a biotite-bearing granitoid from the Suhum basin. No age has been obtained from this sample. Its close proximity and similarity to PK 101 suggests that they belong to the same granitoid. It is therefore likely that 039A has the same age as PK 101.

At the outcrop 039A is a medium to coarse grained biotite-bearing granitoid. It is relatively even grained with some larger K-feldspar phenocrysts. It contains veins and some biotite-rich inclusions that could possibly be derived from its protolith.

5.2.9 PK 101

PK 101 is a biotite- and hornblende-bearing tonalite from the central Suhum basin that has been dated to 2130±10 Ma (Anders Scherstén, unpublished data). Its sample location is close to that of 039A and they probably belong to the same granitoid.

It is weakly foliated and displays dynamic recrystallization through bulging grain boundaries, particularly among quartz, which also exhibit subgrains. It also has epidote-group minerals and metamorphic muscovite.

5.2.10 PK 103

PK 103 is a biotite- and hornblende-bearing granite from the southwestern Suhum basin. It has been dated to 2134±10 Ma (Anders Scherstén, unpublished data).

It is foliated and displays dynamic recrystallization in the form of bulging grain boundaries and subgrains in quartz. It also has epidote-group minerals.

6 Results

6.1 Geochemistry

Results from the chemical analyzes are presented in Appendix A. Based on chemistry and age, the granitoids have been divided into belt and basin types. Selected data and ratios on the belt and basin granitoids are presented in Appendix B, table 1 and 2 respectively.

The samples PK 102, PK 105, 004B, 007A, 019A, 032A and 032B are classified as belt granitoids and PK 101, PK 103, 003A, 003B, 022A, 022D, 022E, 025A, 028A, 028B, 030A, 034A and 039A are classified as basin granitoids.

A subscript $_N$ indicates that the data have been normalized to chondrite values as defined by Boynton

(1984). Likewise, a subscript $_{PM}$ is used for values normalized to the primitive mantle by McDonough *et al.* (1992) (Pr, P, Eu, Dy and Yb from Sun & McDonough 1989). #Mg values are the molar (m/M) [(MgO/(MgO+Fe_2O_3))*100] and A/CNK is the molar [Al_2O_3/(CaO+Na_2O+K_2O)]. Eu-anomalies (Eu/Eu*) were calculated using the formula [$Eu_N/\sqrt{(Sm*Gd)_N}$]. The ferromagnesian content is the sum of Fe_2O_3, MgO, MnO and TiO_2 (wt.%).

The geochemistry of the analyzed samples is presented below. In cases were several samples were taken from the same locality they are presented together.

6.1.1 Belt Granitoids

6.1.1.1 ASGH 004B

004B is sodic with a K_2O/Na_2O of 0.64 and has a high ferromagnesian content (10.93). It also has high #Mg (70.2), Cr_2O_3 (0.020 wt.%) and Ni (49 PPM) relative to the other samples. 004B is metaluminous (A/CNK of 0.92).

It is enriched in LILE compared to HFSE and displays a Ta-Nb through. It has a $(Nb/La)_{PM}$ of 0.30 and a high $(Ce/Pb)_{PM}$ at 1.55 due to a negative Pb-anomaly. The sample has a negative Ti-anomaly (fig. 6).

004B is LREE-enriched and HREE depleted with a $(La/Yb)_N$ ratio of 7.15, $(Gd/Yb)_N$ of 1.75, Yb_N of 9 and a concave shape on the HREE-end ($(Er/Lu)_N$ of 0.92). The curve also displays a small negative Eu/Eu* of 0.95 (fig. 7).

6.1.1.2 ASGH 007A

It has a high silica content (66.54 wt.%), and low ferromagnesian content of 5.42. However, it has relatively high #Mg value of 65. The sample is sodic with a K_2O/Na_2O of 0.43. 007A is weakly metaluminous (A/CNK of 0.97).

It is enriched in LILE compared to HFSE and displays a Ta-Nb through. It has a $(Nb/La)_{PM}$ of 0.20 and a $(Ce/Pb)_{PM}$ of 0.25. 007A has a negative Ti-anomaly.

007A is LREE-enriched and HREE-depleted with a $(La/Yb)_N$ of 11.20, a $(Gd/Yb)_N$ of 1.97 and a Yb_N of 3 (fig. 7). The REE-chondrite curve also display a positive Eu/Eu* of 1.16 that is matched with a positive Sr-anomaly on a primitive mantle normalized diagram (fig. 6). It has low total REE (57.68 PPM).

6.1.1.3 ASGH 019A

019A has the lowest silica-content (56.45 wt.%) and the highest ferromagnesian content (12.0) of the belt granitoids but a relatively low #Mg value of 59. It is sodic with a K_2O/Na_2O of 0.43. 019A is metaluminous (A/CNK of 0.85)

It is enriched in LILE compared to HFSE and displays a Ta-Nb through (fig. 6). It has a $(Nb/La)_{PM}$ of 0.32 and a $(Ce/Pb)_{PM}$ of 0.57. It has a negative Ti-anomaly.

019A is LREE-enriched and HREE-depleted with a $(La/Yb)_N$ value of 5.74, a $(Gd/Yb)_N$ of 1.61 and a Yb_N of 7. It has a very small Eu/Eu*of 0.99 (fig 7).

6.1.1.4 ASGH 032A, 032B

032A has a higher silica content (67.93 wt%) compared to 032B (60.2 wt%) which is otherwise enriched relative to 032A. Consequently, 032A has a lower ferromagnesian content (4.70) compared to 032B (8.13). 032A is more sodic (K_2O/Na_2O of 0.54) compared to 032B (K_2O/Na_2O of 0.63). Both samples have a have a #Mg value of 66. 032A is weakly metaluminous (A/CNK of 0.98) while 032B is metaluminous (A/CNK of 0.86).

Both samples are enriched in LILE compared to HFSE and displays a Ta-Nb. The $(Nb/La)_{PM}$ of 032A is 0.20 and its $(Ce/Pb)_{PM}$ is 0.24. For 032B, the $(Nb/La)_{PM}$ is 0.45 while the $(Ce/Pb)_{PM}$ is 0.27 (fig. 6) Both 032A and 032B display a negative Ti-anomaly.

Both 032A and 032B are LREE-enriched and HREE-depleted. They display very similar REE-curves though 032A is less enriched (total REE 89.76 PPM)

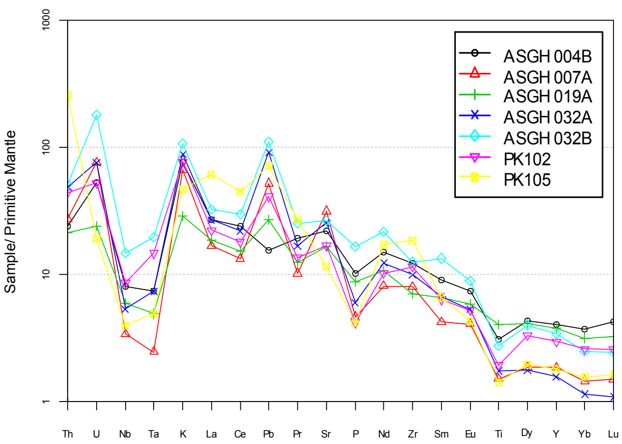

Fig. 6. Primitive mantle-normalized curves for belt granitoids.

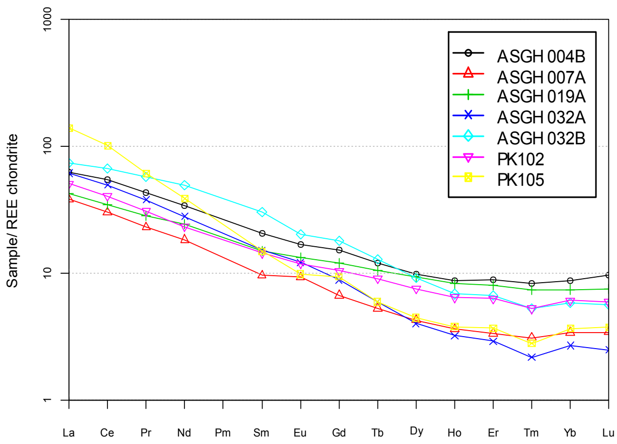

Fig. 7. REE-curves for belt granitoids.

compared to 032B (total REE132.65 PPM) which also has a shallower LREE-slope. 032A has a $(La/Yb)_N$ of 22.9, a $(Gd/Yb)_N$ of 3.29 and a Yb_N of 3. 032A has a $(La/Yb)_N$ of 12.6, a $(Gd/Yb)_N$ of 3.08 and a Yb_N of 6. 032A has a positive Eu/Eu*of 1.05 while 032B has a negative value of 0.87. Both 032A and 032B exhibit a small negative Tm-anomaly (fig. 7).

6.1.1.5 PK 102

The sample has a high silica content (67.55 wt.%) and a low ferromagnesian content (5.64). The #Mg value of PK 102 is 60. It is metaluminous (A/CNK of 0.93) and is sodic with a K_2O/Na_2O of 0.55.

It is enriched in LILE compared to HFSE and displays a Ta-Nb through. It has a $(Nb/La)_{PM}$ of 0.39 and a $(Ce/Pb)_{PM}$ of 0.44 (fig. 6). It also has a negative Ti-anomaly.

PK 102 is LREE-enriched and HREE-depleted with a $(La/Yb)_N$ value of 8.33, a $(Gd/Yb)_N$ of 1.72 and a Yb_N of 6. The sample shows a small negative Eu/Eu* of 0.97 (fig. 7).

6.1.1.6 PK 105

The sample is enriched with the highest silica content (70.34 wt.%) of the belt granitoids and is enriched in LREE with high total REE (165.49 PPM). Its ferromagnesian and #Mg values are the lowest at 4.49 and 53 respectively. It also has a high $(Th/U)_{PM}$ at 13.63 due both its high Th (21.8 PPM) and its low U (0.4 PPM) concentration. PK 105 is metaluminous (A/CNK of 0.96).

PK 105 is enriched in LILE compared to HFSE and displays a Ta-Nb through. The $(Nb/La)_{PM}$ of PK 105 is 0.065 and its $(Ce/Pb)_{PM}$ is 0.62 (fig. 6). The sample also displays a negative Ti-anomaly.

PK 105 is LREE-enriched and HREE-depleted with a $(La/Yb)_N$ value of 38.23, a $(Gd/Yb)_N$ of 2.57 and a Yb_N of 4 (fig. 7). The REE-chondrite normalized curve also displays a negative Eu/Eu* of 0.83 accompanied with a negative Sr-anomaly on a primitive mantle normalized diagram (fig. 6).

6.1.2 Basin Granitoids

6.1.2.1 ASGH 001A

The sample is peraluminous (A/CNK of 1.07) and is the only granitoid that is potassic with a K_2O/Na_2O of 1.10. 001A has an enriched composition, in addition to high total REE it has high Th, Ba, Rb, Pb, Zr, Hf, Nb, Ta concentrations relative to the other samples. The $(Th/U)_{PM}$ is low (0.061) due to a high Th concentration (41.5 PPM).

001A is enriched in LILE compared to HFSE and displays a Ta-Nb through. Its $(Nb/La)_{PM}$ ratio is 0.16, $(Ce/Pb)_{PM}$ is 0.53 and it shows a negative Ti-anomaly (fig. 9).

001A is LREE-enriched and HREE-depleted has a $(La/Yb)_N$ of 59.25, $(Gd/Yb)_N$ of 5.10, Yb_N of 4 and have a high total REE of 321 PPM. It also displays a large negative Eu/Eu* of 0.63 (fig. 10).

6.1.2.2 ASGH 003A, 003B

Both samples are sodic were the K_2O/Na_2O of 003A is 0.22 whereas 003B has a higher value of 0.62. 003A has higher SiO_2, Na_2O, CaO, Sr and U compared to 003B which otherwise is enriched relative to 003A, notably in Ba, Rb, Nb, Zr, Hf and Th. Both samples are peraluminous; 003A has a A/CNK of 1.04 whereas 003B has a value of 1.05.

Both samples are enriched in LILE compared to HFSE and displays a Ta-Nb through. The $(Nb/La)_{PM}$ of 003A is 0.35 while its $(Ce/Pb)_{PM}$ is 0.27. For 003B the $(Nb/La)_{PM}$ is 0.19 whereas the $(Ce/Pb)_{PM}$ is 0.45 (fig. 9). Both samples show a negative Ti-anomaly.

Both 003A and 003B are LREE-enriched and HREE-depleted with $(La/Yb)_N$ of 17.86 and 41.29 respectively. Their $(Gd/Yb)_N$ are 1.88 and 3.55. They have Yb_N of 2 and 3 and total REE of 42.01 and 122.16 respectively. 003A has a large positive Eu/Eu* at 2.16 while 003B has a negative anomaly at 0.95 (fig. 11).

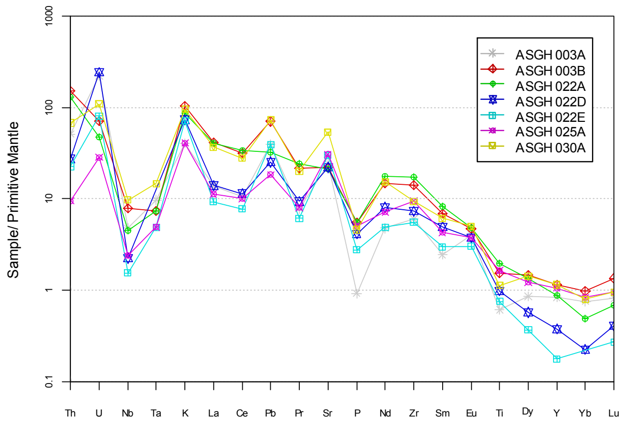

Fig. 9. Primitive mantle normalized curves for basin granitoids.

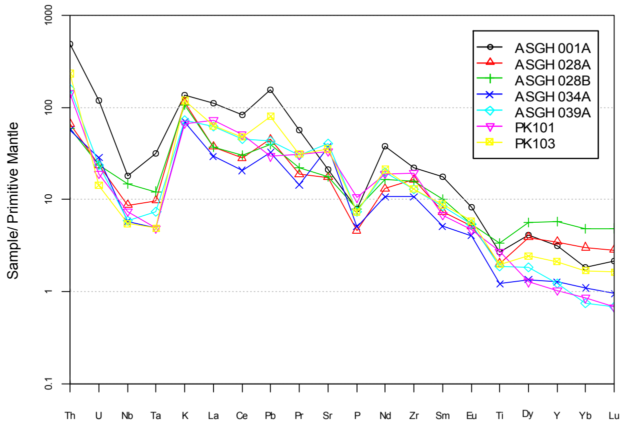

Fig. 8. Primitive mantle normalized curves for basin granitoids.

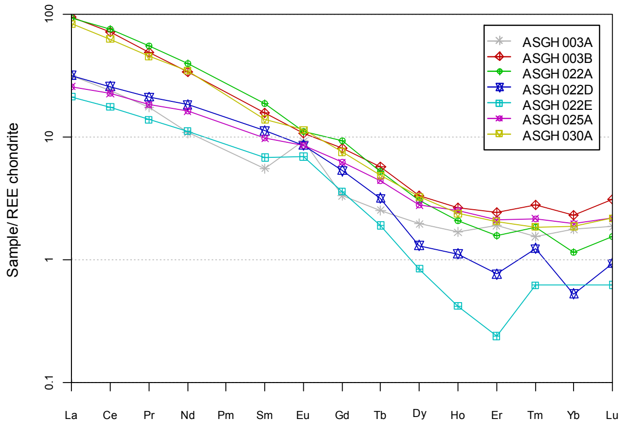

Fig. 11. Chondrite-normalized REE-curves for basin granitoids.

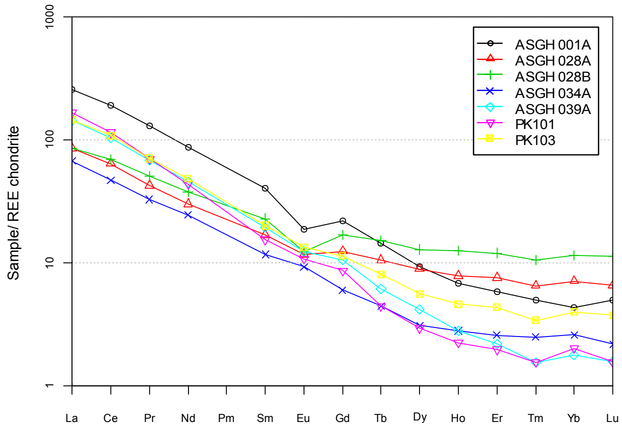

Fig. 10. Chondrite-normalized REE-curves for basin granitoids.

6.1.2.3 ASGH 022A, 022D, 022E

All samples are peraluminous where 022A, 022D and 022E have A/CNK of 1.30, 1.20 and 1.08 respectively. 022A has a less sodic (K_2O/Na_2O of 0.69) compared to 022D and 022E which have lower ratios (0.38 and 0.39). In addition, 022A has higher Ba, Rb, Nb, Ti Hf, Zr, P_2O_5, Th and Fe_2O_3. 022D, and in particular 022E, have higher Sr compared to 022A. They also have higher CaO.

The samples are enriched in LILE compared to HFSE and display a Ta-Nb through. The $(Nb/La)_{PM}$ for 022A, 022D and 022E is 0.11, 0.16 and 0.17 while the $(Ce/Pb)_{PM}$ is 1.04, 0.45 and 0.20 respectively (fig. 9). All samples display a negative Ti-anomaly.

All samples are LREE-enriched and HREE-depleted. 022A has the highest $(La/Yb)_N$ at 80.90 but display the lowest $(Gd/Yb)_N$ at 8.07. Its Yb_N is 1. 022D have lower LREE and is more HREE-depleted with a $(La/Yb)_N$ of 60.68, $(Gd/Yb)_N$ of 10.12 and Yb_N of 1. The Yb value for 022E was below detection limit. However, 022E is more REE-depleted then both 022A and 022D. Total REE for 022A, 022D and 022E is 130.09, 49.57 and 0.38 respectively. The Eu/Eu* for 022A, 022D and 022E is 0.83, 1.11 and 1.40 (fig. 11).

All samples display anomalous Tm and Lu values, these can likely be attributed to analytical uncertainties given the small concentrations of the elements in crustal rocks.

6.1.2.4 ASGH 025A

025A straddles the boundary between metaluminous and peraluminous with an A/CNK of 1.00. It is sodic with a K_2O/Na_2O of 0.24. It has relatively low Ba, Sr, Zr, Hf, Nb and Rb compared to other basin granitoids. It is CaO -rich and displays a positive Sr-anomaly on a primitive mantle-normalized diagram (fig. 9).

The sample is enriched in LILE compared to HFSE and display a Ta-Nb through. Its $Nb/La)_{PM}$ is 0.21, the $(Ce/Pb)_{PM}$ is 0.55 and it displays a negative Ti-anomaly.

The sample is LREE-enriched and HREE-depleted with a $(La/Yb)_N$ of 13.2, a $(Gd/Yb)_N$ of3.17, Yb_N of 2 and total REE of 44.85. The sample has a positive Eu-anomaly of 1.10 (fig. 11).

6.1.2.5 ASGH 028A, 028B

Both samples are sodic; K_2O/Na_2O of 028A is 0.74 whereas 028B has a value of 0.72. Both 028A and 028B are metaluminous (A/CNK of 0.97 and 0.92 respectively). 028A is richer in Ba whereas 028B has higher Rb, Nb and ferromagnesian content.

The samples are enriched in LILE compared to HFSE and display a Ta-Nb through. The $(Nb/La)_{PM}$ of 028A is 0.23, the $(Ce/Pb)_{PM}$ is 0.63. For 028B the $(Nb/La)_{PM}$ is 0.4 while the $(Ce/Pb)_{PM}$ is 0.77 (fig. 8). Both samples display a negative Ti-anomaly.

The samples are LREE-enriched and HREE-depleted. 028A has a $(La/Yb)_N$ of 12.1, a $(Gd/Yb)_N$ of 1.75, Yb_N of 7 and total REE of 116.15. 028B has a $(La/Yb)_N$ of 7.42, a $(Gd/Yb)_N$ of 1.48, Yb_N of 11 and total REE of 131.60. Both samples have a negative Eu/Eu*; 028A has a value of 0.81 while 028B has a value 0.62 (fig. 10).

6.1.2.6 ASGH 030A

030A is weakly metaluminous (A/CNK of 0.98). It is sodic with a K_2O/Na_2O of 0.53 and has positive Sr-anomaly on a primitive mantle-normalized diagram (fig. 9). It has high a Ba concentration (1190 PPM) and a low ferromagnesian content (3.07)

The sample is enriched in LILE compared to HFSE and display a Ta-Nb through. The $(Nb/La)_{PM}$ of 030A is 0.26, the $(Ce/Pb)_{PM}$ is 0.38 and it has a negative Ti-anomaly.

The sample is LREE-enriched and HREE-depleted with a $(La/Yb)_N$ of 44.9, a $(Gd/Yb)_N$ of 4.06, Yb_N of 2 and total REE of 111.37. The sample displays a positive Eu/Eu* of 1.11 (fig. 11).

6.1.2.7 ASGH 034A

It is weakly metaluminous (A/CNK of 0.99) and sodic with a K_2O/Na_2O of 0.40. It displays a positive Sr-anomaly on a primitive mantle-normalized diagram (fig. 8). It has a high Ba concentration (1340 PPM) and a ferromagnesian content of 034A is 3.63.

The sample is enriched in LILE compared to HFSE and display a Ta-Nb through. The $(Nb/La)_{PM}$ of 034A is 0.20, the $(Ce/Pb)_{PM}$ is 0.65 and it has a negative Ti-anomaly (fig. 9).

The sample is LREE-enriched and HREE-depleted with a $(La/Yb)_N$ of 25.97, a $(Gd/Yb)_N$ of 2.32, Yb_N of 3 and total REE of 84.52. The sample has a positive Eu/Eu* of 1.11 (fig. 10).

6.1.2.8 ASGH 039A

It is weakly peraluminous with a A/CNK value of 1.02 and is sodic with a K_2O/Na_2O of 0.47. It displays a positive Sr-anomaly on a primitive mantle-normalized diagram.

The sample is enriched in LILE compared to HFSE and display a Ta-Nb through. It has a $(Nb/La)_{PM}$ of 0.09, a $(Ce/Pb)_{PM}$ of 1.04 and displays a negative Ti-anomaly (fig. 8).

The sample is LREE-enriched and HREE-depleted with a $(La/Yb)_N$ of 80.90, a $(Gd/Yb)_N$ of 5.92, Yb_N of 2 and total REE of 175.35. The Eu/Eu* of 039A is 0.87 (fig. 10).

6.1.2.9 PK 101

PK 101 is weakly peraluminous (A/CNK of 1.01). It is sodic with a K_2O/Na_2O of 0.40. It displays a positive Sr-anomaly on a primitive mantle-normalized diagram but has a negative Ba-anomaly.

The sample is enriched in LILE compared to HFSE and display a Ta-Nb through. The $(Nb/La)_{PM}$ of PK 101 is 0.10 and the $(Ce/Pb)_{PM}$ is 1.71 (fig. 8).

The sample is LREE-enriched and HREE-depleted with a $(La/Yb)_N$ of 82.19, a $(Gd/Yb)_N$ of 4.29, Yb_N of 2 and total REE of 186.91. It has a negative Eu/Eu* of 0.93 (fig. 10).

6.1.2.10 PK 103

The sample is metaluminous with a A/CNK value of 0.93. The sample is sodic but has a high K_2O/Na_2O of 0.92. It also displays high concentrations of Ba and Th relative to other basin granitoids. It displays a positive Sr -anomaly on a primitive mantle-normalized diagram.

The sample is enriched in LILE compared to HFSE and display a Ta-Nb through. The $(Nb/La)_{PM}$ of PK 103 is 0.09, the $(Ce/Pb)_{PM}$ is 0.60 and it has a negative Ti-anomaly (fig. 8).

The sample is LREE-enriched and HREE-depleted with a $(La/Yb)_N$ of 36.47, a $(Gd/Yb)_N$ of 2.86, Yb_N of 4 and total REE of 182.41. It has a negative Eu/Eu* of 0.88 (fig. 10).

7 Discussion

7.1 Petrogenesis of belt granitoids

7.1.1 Tectonic setting and source

All belt granitoids display a decoupled LILE-HFSE pattern (fig. 12) as well as low $(Nb/La)_{PM}$ and, with the exception of 004B, low $(Ce/Pb)_{PM}$. These values are consistent with a subduction setting (Kemp & Hawkesworth 2003). The high $(Ce/Pb)_{PM}$ displayed by 004B is the result of a negative Pb-anomaly, which may be the result of either a Pb-poor source or Pb-loss subsequent to emplacement of the granitoid.

On Rb-Y-Nb and Rb-Yb-Ta discrimination diagrams by Pearce *et al*. (1984) all belt granitoids plot in the volcanic arc granitoid (VAG) fields (fig. 13). While diagrams such as these do not make a distinction between island or continental arcs, it reinforces the interpretation that emplacement of the granitoids took place in a subduction setting.

However, even though the granitoids have formed in the same tectonic setting the differences in for example REE-enrichment or ferromagnesian content indicate that they have not formed from the same source. This suggests temporal and/or spatial changes in subduction style.

All granitoids show LREE-enrichment ((La/Yb_N between 5.74-38.23) and HREE-fractionation ($(Gd/Yb)_N$ of 1.61-3.29). HREE-fractionation indicates that garnet was a stable phase in the source. In addition, 004B display a concave HREE-end. Such a shape could result from fractionating amphibole as it has its highest partition coefficients for MREE (Rollinson 1993).

The negative Tm-anomalies that can be seen among 007A, 032A, 032B, PK 102 and PK 105 can be attributed to analytical uncertainties since Tm occur in small concentrations in crustal rocks, making it hard to analyze (Rollinson 1993; Anders Scherstén, personal

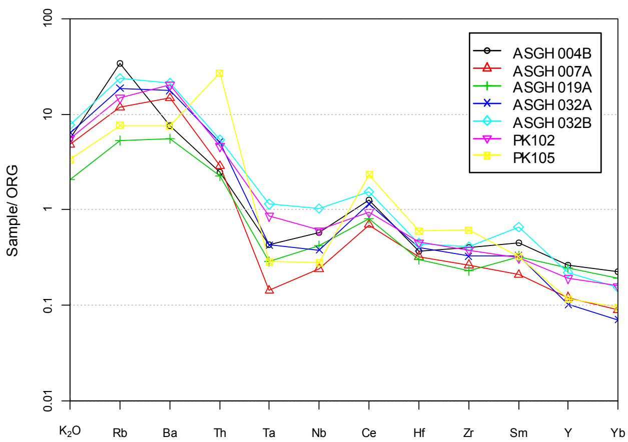

Fig. 12. Belt granitoids normalized to ORG by Pearce *et al.* (1984).

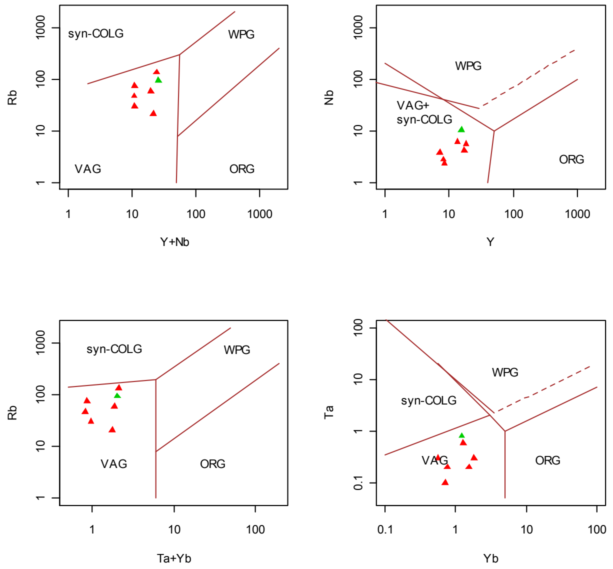

Fig. 13. Rb-Y-Nd and Rb-Yb-Ta diagrams by Pearce *et al.* (1984). All belt granitoids plot within the VAG field. Green triangle is 032B.

communication).

The control of plagioclase on Sr and Eu can be seen on a Sr/Nd-Eu/Eu* diagram (fig. 14) where the samples show a positive correlation. The small anomalies of 004B, 019A and PK 102 show that plagioclase has been present as a residual or fractionating phase but have not exerted a major control on the melt. Since plagioclase crystallize early in melts the absence of a Eu/Eu* indicates that these granitoids are relatively unmodified by crystal fractionation.

The negative Eu/Eu* of PK 105 may at least in part be the result of a positive Gd-anomaly (fig. 7). However, it also displays a negative Sr-anomaly indicating that plagioclase was a residual or fractionating phase. The positive Eu/Eu* and Sr-anomaly of 007A can result from three processes: First, it could be derived from a plagioclase-rich source. Secondly, the melt could have been generated in a water-saturated environment where the stability of plagioclase became suppressed against hydrous minerals. Finally, it could represent a cumulate that has been enriched in plagioclase during crystal fractionation (Tarney & Jones 1994; Kemp & Hawkesworth 2003). 032A and 032B represent a special case since 032B occur as enclaves within 032A (see discussion below). However, their relationship suggests that the anomalies are the result of fractional crystallization.

Whether these anomalies are the result of fractionating phases in the residue or during crystallization have important implications for how the source is interpreted. On a Harkers variation diagram (fig. 15) for major elements vs. SiO_2 the granitoids show a negative correlation between Al_2O_3, MgO, CaO, FeOt, TiO_2 and P_2O_5 with increasing SiO_2, whereas it has a less clear but positive correlation with Na_2O and K_2O. Such a correlation could arise from fractional crystallization of magma with a composition similar to 019A (low SiO_2). Also, the matching Eu/Eu* of 032A and 032B (discussed below) indicate that fractional crystallization has occurred. As a consequence, the Eu/Eu* of 032A, 032B and PK 105 might be partly derived from fractional crystallization.

Contamination and mixing have to be taken into account when considering the composition of the granitoids; 007A (and possibly 019A) contain basaltic inclusions - probably derived from volcanic rocks in the greenstone belts - while the relationship between 032A and 032B strongly suggests mixing of magmas (see below).

No chemical analyzes is available on the basaltic inclusion of 007A. However, Dampare *et al.* (2008) performed analyzes on basalts and andesites from the southern Ashanti belt at localities close to 007A. REE-chondrite normalized curves varied from flat or LREE-depleted (basalt) to LREE-enriched and HREE depleted (andesite). Dacites analyzed by Sylvester and Attoh (1992), also from the southern Ashanti belt, show LREE -enrichment and HREE-depletion. The effect of contamination on a granitoid such as 007A from flat or REE-depleted basalt would be to “level out” the REE-curve making it appear both less LREE-enriched as well as HREE-depleted. In addition, contamination from mafic rocks could also raise the ferromagnesian content of the melts. The impact of felsic rocks such as dacites or andesites during contamination should be less given their compositional similarity to the granitoids.

The field relationships of 032A and 032B indicate that they are genetically linked, probably through mixing

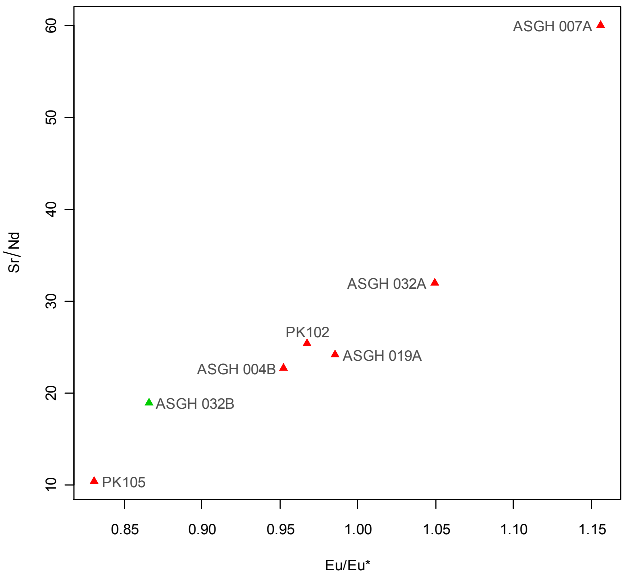

Fig. 14. Sr/Nd and Eu/Eu* show a positive correlation. The behavior of Sr and Eu is controlled by plagioclase which has high partition coefficients for both elements.

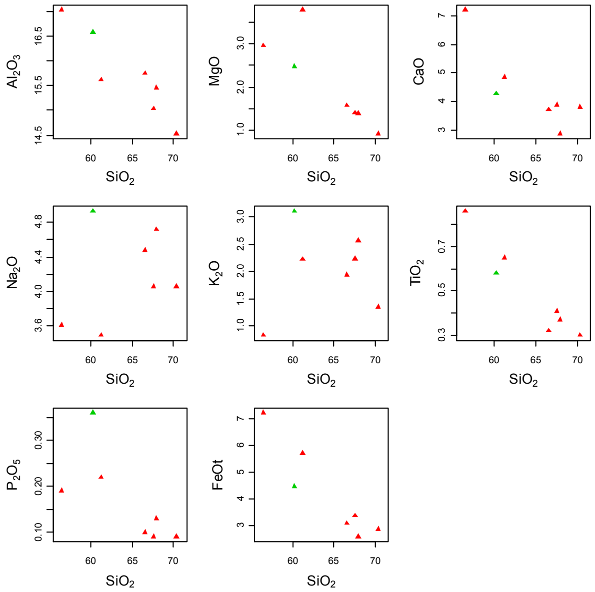

Fig. 15. Harker variation diagram for belt granitoids. 032B is marked in green.

(Anders Scherstén, personal communication). The shapes of their REE-curves are very similar although 032B is more enriched (fig. 7) A positive Eu/Eu* of 032A (1.05) is matched by a negative Eu/Eu* of 032B (0.87). This would suggest that 032B is an evolved melt derived from fractional crystallization of 032A. However, 032B has a lower SiO_2 content than 032A but is otherwise enriched in all major elements. This is a pattern that is hard to reconcile with a model of fractional crystallization. Instead, it supports the interpretation that 032B is the result of mixing between 032A and a late injection of magma.

The higher ferromagnesian content of 032B (8.13) compared to 032A (4.70) indicates that this magma was more juvenile. Assuming that the positive Eu/Eu* of 032A indicates that it acted as a cumulate, then the evolved melt that the juvenile magma mixed with would have been enriched in REE and have a negative Eu/Eu*. The shallower LREE-end of 032B indicates that the new magma had a lower LREE content. The occurrence of 032B as small rounded enclaves within 032A could be explained through a density contrast. The higher ferromagnesian content of 032B means that its density is higher compared to 032A. Upon mixing blobs of 032B would therefore have sunken into 032A until a neutral density contrast was reached. Mixing must therefore have occurred before 032A crystallized.

Among the belt granitoids PK 105 have a conspicuously high concentration of Th. Hawkesworth *et al.* (1997) argued that in subduction zones high Th, and as a consequence low U/Th and Ba/Th, was an indicator of a sedimentary contribution to the melt. U (particularly when oxidized) and Ba are LILE and highly mobile in fluids. During dehydration of a subducting slab they are expected to be mobilized and transported into the overlying mantle. However, Th acts as a HFSE and therefore remains in the slab during dehydration. As a result, granitoids formed from dehydration of a slab and subsequent melting of the mantle are expected to have high U/Th and Ba/Th. Hawkesworth *et al.* (1997) suggested that low U/Th and Ba/Th were the result of direct melting of Th-rich sediment in the slab, an argument they also supported with isotope data. In addition, Hawkesworth *et al.* (1997) also used Th/Ce as an indicator of a sediment contribution to the melt. Ce is mobile in fluids and in normal subduction zones, were only dehydration of the slab occurs, the ratio should accordingly be low. However, in slab melts, were HFSE such as Th are incorporated the ratio will be higher (Hawkesworth *et al.* 1997).

Hawkesworth *et al.* (1997) used Ba/Th-Th and U/Th-Th diagrams to illustrate the varying contribution of slab melts. On such diagrams (fig. 16) PK 105 plots on low Ba/Th and U/Th but high Th compared to the other belt granitoids. The low values are partly an effect of low Ba and U concentrations but mostly its high Th concentration. Such a high Th concentration could be explained with a sedimentary component in PK 105, which would be lacking in other belt granitoids.

High Ba/Th and U/Th and low Th/Ce is most common in depleted island arcs while low Ba/Th and U/Th and high Th/Ce is found in more evolved arcs where the sediment flux can be expected to be higher (Hawkesworth *et al.* 1997; Kemp & Hawkesworth 2003). A possible implication of this would be that PK 105 was emplaced in a more evolved island arc compared to the remaining belt granitoids. In addition, PK 105 also show high LREE compared to the other granitoids. This may be derived from crustal contamination or from enriched sediment brought into the subduction zone. High K_2O/Na_2O and LREE contents in basin granitoids (001A, 039A, PK 101 and PK 103) from southeastern Ghana may indicate the extent of such an evolved arc.

However, the enriched composition of PK 105 could also be the result of small degree melting coupled with fractional crystallization leading to enrichment of incompatible elements. Rb-Sr and Sm-Nd isotopic studies could constrain any possible sedimentary contribution to PK 105 (Hawkesworth *et al.* 1997).

7.1.2 Are belt granitoids TTGs?

The belt granitoids show many similarities to TTGs. They are relatively sodic and have been derived from a source with stable garnet but little plagioclase. In addition, the association between the belt granitoids and surrounding greenstone belts is reminiscent of Archean terranes were TTGs form bimodal suites together with high-Mg basalts (Kemp & Hawkesworth 2003).

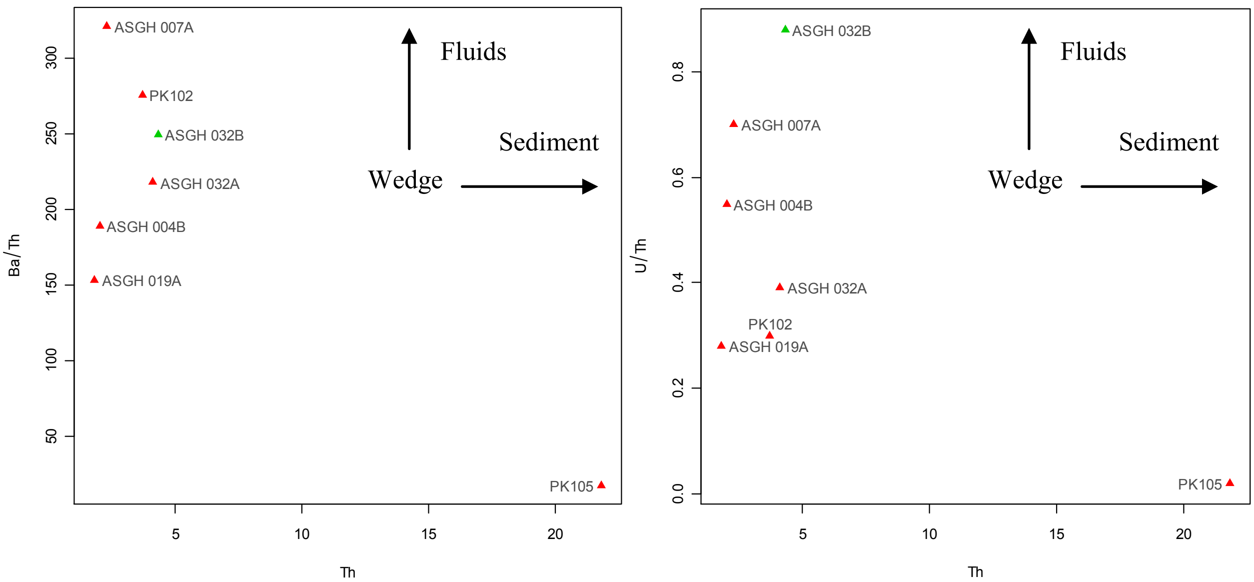

Fig. 16. During dehydration of a subducting slab Ba and U are discoupled from Th. This yields high Ba/Th and U/Th in the fluids and subsequent melt. Melting of sediment in the slab incoorporates Th and thus yields low ratios. Diagrams and trends by Hawkesworth *et al.* (1997).

7.1.2.1 First things first, what are TTGs?

TTGs (tonalite-trondhjemite-granodiorite) suites are a major component of Archean terranes, comprising as much as 90% of the Archean continental crust (Martin *et al.* 2005). The petrogenesis of TTGs is controversial; some authors argue that they are mainly generated in subduction zones through partial melting of a subducting slab (Martin 1993; Foley *et al.* 2002; Martin *et al.* 2005) while others believe that they originate as basal partial melts of thickened oceanic crust (Condie 2005). Either way, the source is considered to be hydrated basalt melted in either amphibolite or eclogite-facies conditions (Kemp & Hawkesworth 2003; Martin *et al.* 2005).

Martin *et al.* (2005) defined TTGs as Si-rich (SiO_2> 64 wt.%) granitoids with a high Na concentration (3-7 wt.%), a K_2O/Na_2O below 0.5 and a ferromagnesian content of less than 5 wt.%. In addition, high REE fractionation ($(La/Yb)_N$ between 5-150 according to Martin 1993) is considered characteristic of TTGs and is attributed to residual garnet and amphibole (Martin 1993). Unlike Post-Archean granites, TTGs do not display potassium enrichment during fractional crystallization (Martin 1993). TTGs often have concave HREE-ends, implying that amphibole (which has its highest partition coefficient for MREE) is a common residual phase (Martin 1993).

A compilation of TTGs by Kemp and Hawkesworth (2003) had Eu/Eu* mainly in the range of 0.8-1.2 but their average TTG (n=355) had a value of 1.037. The general lack of significant negative anomalies indicates that plagioclase is not a major mineral in the residue of TTGs (Kemp & Hawkesworth 2003). Positive anomalies have been attributed to melting in water-saturated conditions (Tarney & Jones 1994).

TTG-like rocks are rarely encountered in Post-Archean terranes. This is believed to be a direct result of a continuously lowered geotherm when the earth cooled. As partial melting of basalt requires high temperatures a lowered geotherm effectively prevented formation of TTGs (Martin *et al.* 2005).

Adakites, considered by some to be a modern equivalent of TTGs, are mostly encountered in areas were young crust or oceanic ridges are being subducted, as these are warm enough to facilitate partial melting (Defant & Drummond 1990; Martin *et al.* 2005). However, adakites are also believed to have formed from partial melting of the crust due to upwelling asthenospheric mantle following delamination of the lithosphere (Condie 2005). Martin *et al.* (2005) argued that the close similarities between a certain type of adakites, formed in subduction zones, and late Archean TTGs indicated that the latter originated in the same environment.

Martin and Moyen (2002) showed that TTGs underwent secular changes between 4.0-2.5 Ga. They found that Sr, Ni, Cr and #Mg increased in the least fractionated rocks. They argued that this reflected an increasingly steeper angle of subduction, in turn reflecting a cooling earth. Steeper subduction would have meant that the interaction between slab melts and mantle peridotite would have increased over time. Such interaction would explain the rise in #Mg, Ni and Cr. Increasing Sr was attributed by Martin and Moyen (2002) to melting below the stability field of plagioclase, another result of steeper subduction. However, it could also reflect smaller degrees of melting (Kemp & Hawkesworth 2003).

These changes reflect how partial melting became less important in subduction zones over time. Instead, dehydration of the subducting slab and hydration of the overlying mantle, which would subsequently act as the melt source, became more common (Martin *et al.* 2005).

Sanukitoids, believed to result from melting of a mantle metasomatized with a partial melt from the slab, represent an intermediate between the two processes. As slab melts, which are felsic, are not in equilibrium with the mantle they will begin to react with each other. The melt/mantle ratio therefore determines whether the melt is consumed in reactions with the mantle or if it reaches the crust. The depth of melt generation, and thus the distance the melt have to travel through the mantle, also has importance (Martin *et al.* 2005).

7.1.2.2 So where do the belt granitoids fit in?

When using the definition of Martin *et al.* (2005) only PK 105 qualifies as a true TTG. 007A and 032A have somewhat higher ferromagnesian and K_2O/Na_2O values respectively but otherwise also qualify. The remaining granitoids are either more ferromagnesian, have lower silica content or to high K_2O/Na_2O. This would suggest that the granitoids not only consists of a slab melt but also contain other components.

Martin *et al.* (2005) identified two types of adakites: the low silica adakite (LSA) (<60 wt.%) and the high silica adakite (HSA) (>60 wt.%). The compositional differences between LSA and HSA were attributed to an increasing degree of mantle interaction from the HSA to the LSA. The LSA shows a composition that overlaps with sanukitoids while the HSA have a composition like TTGs. Martin *et al.* (2005) used a ternary (SiO_2/MgO) *100-Sr-K/Rb diagram to illustrate differences between the LSA and HSA.

The SiO_2/MgO on a (SiO_2/MgO)*100-Sr-K/Rb diagram (fig. 17) is meant to illustrate the degree of interaction between the melt and the mantle were higher MgO is found in LSA compared to HSA (Martin *et al.* 2005).

Melting of a basaltic source (assumed to be a good approximate of the source of HSA) below the stability field of plagioclase can only, due to its low Sr concentration, yield melts with up to 1000 PPM Sr. However, melting of peridotite, metasomatized with a slab melt, can give melts with a Sr concentration up to 2500 PPM. LSA therefore have higher Sr compared to HSA rocks (Martin *et al.* 2005).

Finally, Martin *et al.* (2005) noted that higher K/Rb ratios occurred in LSA compared to HSA. They attributed this to selective melting of amphibole in metasomatized mantle peridotite. During melting of a basaltic source (as is the case of HSA) the partition coefficients of the residual minerals (garnet, amphibole or clinopyroxene) would instead impart a low ratio on the melt.

On the (SiO_2/MgO)*100-Sr-K/Rb diagram the belt granitoids form a trend from high SiO_2/MgO towards higher Sr and K/Rb (fig. 17). This can be interpreted as an increasing interaction with mantle peridotite. Indeed, the granitoids (004B, 019a and 032B) who display a composition with high Sr, ferromagnesian, Ni, Cr_2O_3 and #Mg are also the ones that plot closest to the LSA field. PK 105 on the other hand plots close to the SiO_2/MgO, apex in accordance with its TTG-affinity.

This diagram illustrates that the granitoids show a close association with the HSA of Martin *et al.* (2005), indicating that they originated as slab melts. However, it also illustrates a trend in which the slab melts increasingly begin to interact with the mantle. A consequence is that the angle of subduction, perhaps in association with the volume of melt being generated, must have varied between the granitoids.

Barker and Arth (1976) used a ternary Na-K-Ca (molar) diagram to distinguish calc-alkaline rocks from TTG suites. As shown in figure 18, calc-alkaline rocks have a differentiation trend that goes towards increasing K_2O. This is not seen among TTGs which do not show K_2O-enrichment during differentiation. Instead, they move towards higher Na_2O (Barker & Arth 1976).

When plotting basin and belt granitoids, from this work and from Doumbia *et al.* (1998), they define a differentiation trend similar to the calc-alkaline (CA, fig. 18) This is characteristic of LSA and sanukitoids whereas HSA (and by definition TTG) should show a trondhjemitic differentiation trend (Td, fig. 18). The granitoids also plot in the field of sanukitoids in figure 19 from Martin *et al.* (2005). Basin granitoids have higher K_2O compared to belt granitoids, this is to be expected given that they comprise reworked crust (see section 7.2) compared to the more juvenile source of the belt granitoids.

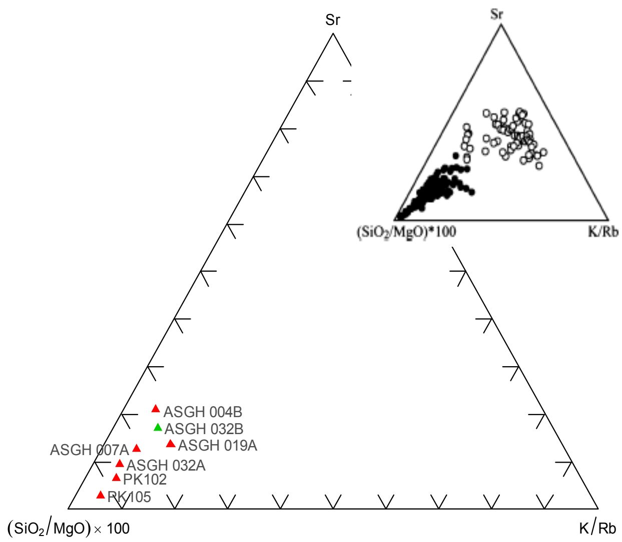

Fig. 17. The belt granitoids show increasing mantle interaction leading to higher Sr and K/Rb. Inserted diagram show the position of HSA (filled circles) and LSA (open circles). Diagrams from Martin *et al.* (2005)

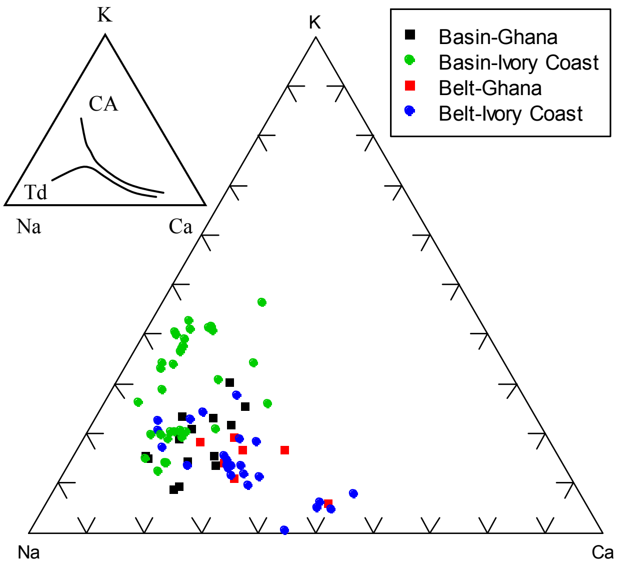

Fig. 18. Belt and basin granitoids from Ghana (this thesis) and the Ivory Coast (Doumbia *et al.* 1998). Belt granitoids follow a differentiation trend intermediate between the trondhjemitic (Td) and calc-alkaline trend (CA). Na-K-Ca diagram and trends from Barker and Arth (1976).

In figure 20 Birimian granitoids from Ghana (this work), the Ivory Coast (Doumbia *et al.* 1998), the Reguibat shield (Boher *et al.* 1992), the Kedougou-Kenieba inliers (Boher *et al.* 1992) and the Baoulé Mossi (Boher *et al.* 1992) have been plotted together. As in figure 18 they define a calc-alkaline path. Even though Boher *et al.* (1992) did not make a distinction between belt and basin types the data from Doumbia *et al.* (1998) and this thesis show that belt granitoids are confined to lower K_2O whereas basin granitoids have higher values. The same trend can therefore be assumed to apply to the granitoids of Boher *et al.* (1992).

Some regional differences can be seen in figure 20 where granitoids from the Reguibat shield appear to have higher K_2O. However, this could also be a result of sampling primarily of basin type granitoids by Boher *et al.* (1992).

It is apparent that granitoids from across the Birimian terrane follow the same trend as those from Ghana and the Ivory Coast. Collectively the Birimian granitoids do not define any clear trondhjemitic differentiation trend, even though a few outliers may indicate that there are some true TTGs present in the Birimian terrane (fig. 20).

An average TTG from Kemp and Hawkesworth (2003) has also been plotted in figure 20 were it occur together with the belt granitoids. This is probably an effect of the value being an average, therefore plotting in the middle of the trondhjemitic differentiation path which, at that point, crosses the calc-alkaline path. However, this helps to explain the apparent TTG-affinity of the belt granitoids, especially PK 105.

It is unlikely that the granitoids are analogous to the calc-alkaline Archean granites of Kemp and Hawkesworth (2003). These formed through intracrustal melting of Archean crust and have many characteristics believed to be inherited from TTGs. However, average calc-alkaline granites of Kemp and Hawkesworth (2003) have lower #Mg and higher K_2O compared to the belt granitoids (fig. 20). Also, their TTG-like composition still requires that TTGs were present in their source. The lack of true TTGs, evident in figure 20, therefore suggests that a scenario with infracrustal melting yielding TTG-like calc-alkaline granites is an unlikely model for the belt granitoids.

Sylvester and Attoh (1992) has also suggested that some volcanics in Ghana have characteristics of sanukitoids.

Even when assuming that the granitoids formed in a subduction setting were slab melting was an important part, the behavior of the belt granitoids still leaves some confusion regarding how to best classify them. On

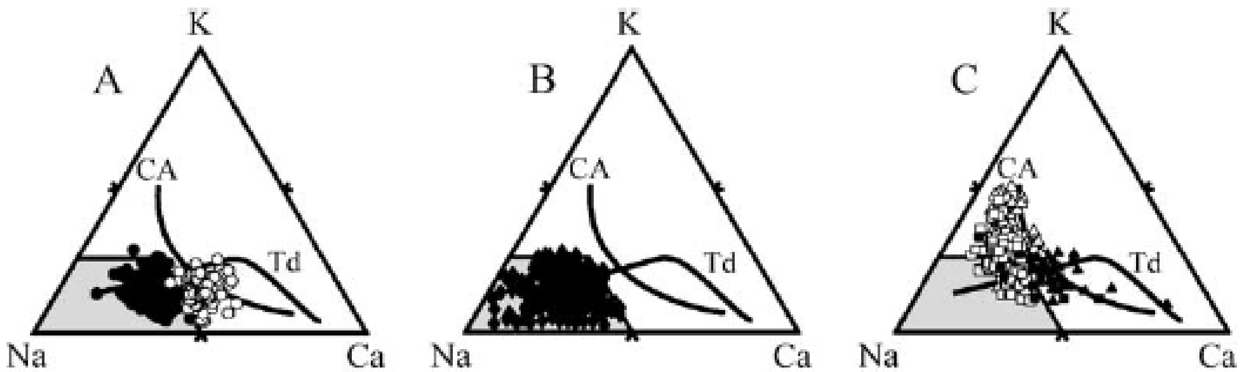

Fig. 19. Na-K-Ca diagrams showing the location of: A) HSA, black circles, LSA, white circles; B) TTGs; C) Sanukitoids (squares) and Closepet granitoids (triangles). Black symbols are less then 62 wt.% silica, white are over 62 wt.%. Closepet granitoids are similar petrogenetically to sanukitoids and Martin *et al.* (2005) therfore plotted them together. The grey field represent the area in which TTGs plot. From Martin *et al.* (2005).

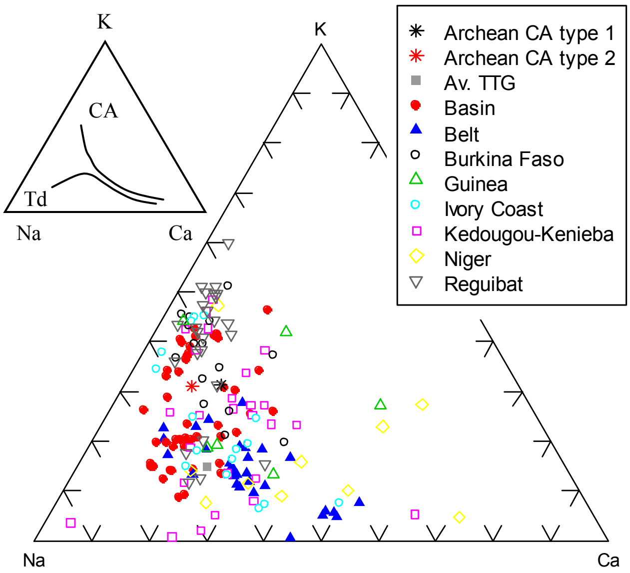

Fig. 20. Na-K-Ca diagram with Birimian granitoids from the West African Craton and average TTG and Archean calc-alkaline granitoids. See text from discussion. Average TTG and Archean calc-alkaline granites from Kemp and Hakwesworth (2003). Basin and belt granitoids are from Ghana (this thesis and the Ivory Coast (Doumbia *et al.* 1998). Other Ivory Coast granitoids (open green circles) and granitoids from Guinea, Kedougou-Kenieba, Niger, Burkina Faso and Reguibat are from Boher *et al.* (1992). Na-K-Ca diagram and trends from Barker and Arth (1976).

the (SiO_2/MgO)*100-Sr-K/Rb they show a composition in line with HSA (or TTG). Neither do they contain pyroxenes which may be encountered in LSA and sanukitoids (Martin *et al.* 2005). Meanwhile, on the Na-K-Ca diagram they show a behavior similar to LSA and sanukitoids.

The granitoids contain a slab melt component which accounts for their TTG-like character. However, they also show a calc-alkaline behavior and signs of mantle interaction (although variable). Even though they cannot be classified as TTGs their slab melt contribution needs to be recognized. Doumbia *et al.* (1998) used the term sodic calc-alkaline for belt granitoids in the Ivory Coast. Such a term may perhaps be suitable since it recognizes both the slab melt component as well as the granitoids calc-alkaline character.

7.1.3 Spatial and temporal changes among the belt granitoids

The belt granitoids were emplaced between 2232-2170 Ma (Anders Scherstén, unpublished data). With the exception of PK 102 the granitoids show a trend of decreasing ages towards the northwest. This is a trend that has previously been noted by Hirdes *et al.* (1996) and Hirdes and Davis (2002).

PK 102 occurs in the Suhum basin, approximately 20 kilometers north of PK 105. However, the granitoid is 52 Ma younger. Two implications follow on this:

First, assuming that both granitoids were emplaced in a subduction setting, it means that it must have been active between at least 2232-2180 Ma and as a consequence, accretion of terranes from the northwest, following the model of Feybesse *et al.* (2006), must have occurred after this period.

Secondly, the $(La/Yb)_N$ and $(Ga/Yb)_N$ decreases from PK 105 to PK 102. This indicates that garnet became less important in the source over time. This can be taken to reflect an increased angle of subduction, and thus cooler oceanic crust, were slab-melting became less important. The ferromagnesian content and #Mg of PK 102 is also higher. This may indicate increased mantle interaction.

The ages of PK 102 and PK 105 in the Suhum basin overlaps with ages from the Kibi-Winneba, Ashanti and Sefwi belts (Appendix C). Magmatic activity must therefore have been partly coeval between the belts, even though it started earlier in the southeast.

007A is ~2 Ma younger then 004B (table 1) but show compositional differences where 004B is more juvenile and has lower $(La/Yb)_N$. This suggests that 004B contains a smaller slab melt component compared to 007A.

Mixing between 032A and the juvenile magma that formed 032B probably occurred at a late stage when 032A had already begun to undergo crystal fractionation (see discussion above). The juvenile magma may have originated from the same source as 032A but as a late small-degree melt. Its high ferromagnesian content could partly reflect a more unfractionated nature but could also be the result of increased reaction with the mantle.

On a $(La/Yb)_N$-Yb_N diagram (fig. 21) the granitoids form a trend that goes from the Archean TTG field defined by Martin (1987, cited by Martin 1993) to where it overlaps with Proterozoic granitoids. This field corresponds in time to approximately 2.5-2.2 Ga (Martin 1993). Such a relationship was also noted by Sylvester and Attoh (1992) in volcanic rocks from the Kibi-Winneba, Ashanti and Bole-Navrango belts (fig. 2). Such a trend is to be expected given the composition of the granitoids, falling between TTGs generated by slab melts and Post-Archean styled subduction processes where melts are generated by fusion of hydrated mantle.

7.2 Petrogenesis of basin granitoids

7.2.1 Tectonic setting

Basin granitoids show a higher degree of variance compared to belt granitoids. They comprise leucocratic granites (*sensu strictu*), two-mica granitoids (muscovite and biotite), biotite-granites (*sensu strictu*) and biotite-hornblende granitoids. They are more felsic then belt granitoids with silica contents varying between 63.9-72.65 wt.% and ferromagnesian values between 2.28-

6.82. Compositions range from metaluminous to peraluminous with A/CNK between 0.92-1.08. Among the basin granitoids $(La/Yb)_N$ varies between 7.42-82.2 and $(Gd/Yb)_N$ between 1.48-10.2.

Like the belt granitoids the basins granitoids show a trend of younging towards the northwest, in accordance to what was observed by Hirdes *et al.* (1996) and Hirdes and Davis (2002). The only exception to this pattern is 001A from the Winneba granitoid. Since no ages are available from 030A and 034A it is not possible to say whether the younger age of the Winneba granitoid is a local feature or if it applies to the entire Kibi-Winneba belt.

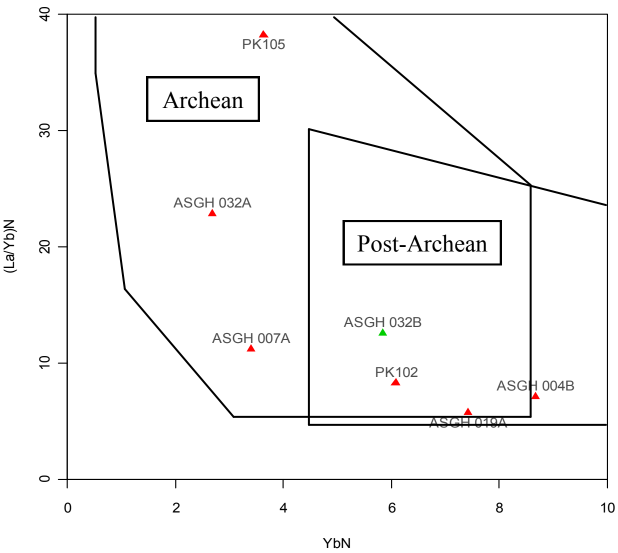

Fig. 21. $(La/Yb)_N$-Yb_N diagram in which belt granitoids show a transitional trend plotting both in the archean and post Archean fields. Diagram and fields from Martin (1993).

The basin granitoids are considered to have formed through crustal anatexis (e.g. Feybesse *et al.* 2006). Many of the general characteristics of the basin granitoids, such as REE fractionation, decoupled LILE-HFSE and a Nb-La through, can most easily be explained by being inherited from the magmatic rocks of the greenstone belts.

Variations among the belt granitoids are also reflected in the basin granitoids. In the Suhum basin, 039A, PK 101 and PK 103 have high LREE and Th similar to PK 105. In the same way 028A and 028B have low Th, reflecting a composition more similar to PK 102 while in the Kibi-Winneba belt 030A and 034A are similar to 032A. Relationships are less clear between basin granitoids in the Sunyani, Kumasi and Cape Coast basins and the belt granitoids in adjacent greenstone belts, possibly as a result of being further away from the belt granitoids.

The high degree of HREE-fractionation displayed by some basin granitoids cannot be explained with inheritance alone since it is considerably higher then what is seen among belt granitoids (highest $(Gd/Yb)_N$ is 3.29). Samples that display a "higher then belt granitoid" $(Gd/Yb)_N$ are 001A, 003B, 022A, 022D, 022E, 030A, 039A and PK 101. The high HREE-fractionation is most easily explained by garnet being a stable phase in the residue.

The presence of garnet would indicate that these rocks were sourced from deep crustal levels. HREE-fractionation may also be the result of residual accessory phases such as zircon (Rollinson 1993). However, that would mean that such accessory phases were only important in the residue of some basin granitoids.

The basin granitoids can, based on mineralogy and composition, be divided into five groups: leucocratic granites, two-mica granitoids, biotite granitoids, biotite-hornblende granitoids and the Winneba granitoid (001A).

7.2.1.1 Leucocratic granites

Leucocratic granites (004A, 004C, 004D, 022C and 025B) occur as veins that crosscut both basin (022A, 022D, O22E and 025A) and belt (004B) granitoids. Assuming that they are related to the same event intrusion of leucocratic granites must therefore have occurred during the late stage of the Eburnean orogeny following intrusion and crystallization of 025A. This is supported by the age of 022C which is, within error, the same as 022A (Anders Scherstén, personal communication – appendix C: table 1).

No chemical analyzes are available on the leucocratic granites and it is thus not possible to constrain their petrogenetic relationship to the granitoids they intrude. However, since they occur as veins and not large plutonic bodies any melting taking place must have occurred at a relatively small scale. A reasonable explanation for their origin is that the leucocratic veins represent late-stage evolved residual melts that intruded into surrounding rocks, either along preexisting structures or through fractures created by hydraulic fracturing. Another possibility could be that they are associated with small-scale melting during thermal relaxation following the Eburnean orogeny.

7.2.1.2 Two-mica, biotite and biotite-hornblende granitoids

The two-mica, biotite and biotite-hornblende granitoids are the three main types of basin granitoids. Two-mica granitoids are peraluminous with A/CNK between 1.00-1.20 while the biotite and biotite-hornblende granitoids are metaluminous to weakly peraluminous with A/CNK between 0.92-1.02.

Two-mica granitoids occur in the Cape Coast (003A and 003B), Sunyani (022B – see Appendix B, 022D and 022E) and Kumasi (025A) basins. In Sunyani the two-mica granites coexist with 022A, a biotite-hornblende bearing granitoid. In the Sunyani basin the distribution of biotite and muscovite is relatively even while biotite dominates in the Cape Coast and Kumasi basins. Biotite and biotite-hornblende granitoids occur in the Suhum basin (028A, 028B, 039A, PK 101 and PK 103), the Kibi-Winneba belt (030A and 034A) and Sunyani basin (022A).

Many of the granitoids have characteristics of migmatites. This is especially evident among 022A, 022D and 022E. Their REE-curves show similar shapes (fig. 22a) although 022D and 022E are more depleted and have increasingly fractionated HREE. The samples display a complementary behavior; 022A have high A/CNK, K_2O/Na_2O, Ba, Rb, Nb, Ti, P, Th, Hf, Zr, and La but low Sr and Eu/Eu*. This is complimented by 022D and 022E who show the opposite behavior with high Sr and Eu/Eu* but lower values of the other elements (fig. 22b). They also have higher U then 022A. In terms of concentrations 022D assume an intermediate position between 022A and 022E. The Tm and Lu-anomalies can be attributed to analytical uncertainties. The mafic composition of 022A compared to the more felsic composition of 022D and 022E indicate that the latter are leucosomes whereas the former is the residue.

What does this mean? The fact that 022A has higher K_2O/Na_2O, Ba, Nb, Ti, Zr, Hf, P and suggests that K-feldspar, biotite, zircon and apatite has been stable during melting (Kemp & Hawkesworth 2003). The rising Eu/Eu* and Sr and decreasing A/CNK of 022D and 022E also indicates that plagioclase was a major contributor to the melt (Patiño Douce & Harris 1998).

High Sr and Eu/Eu* could also be achieved through accumulation of plagioclase during crystal fractionation. In such a case the positive Eu/Eu* of 022D and 022E would be acheived by accumulation of plagioclase leaving a residual melt with a negative Eu/Eu*. The mafic mineral assemblage of 022A means it cannot have crystallized from such a residual melt. Instead, a model in which 022D and 022E are plagioclase cumulates requires an additional felsic leucosome with a negative Eu/Eu*.

Such a lecuosome has not been found and the relationship between 022A, 022D and 022E therefore inidcates that 022D and 022E were derived from preferential melting of plagioclase, leaving 022A as a residue.

Preferential melting of plagioclase can occur in water-saturated conditions were hydrous minerals such as biotite are stabilized (Patiño Douce & Harris 1998; Kemp & Hawkesworth 2003). As a result plagioclase would contribute both Sr and Eu to the melt, explaining the higher Sr and Eu/Eu* found in 022D and particularly 022E (Patiño Douce & Harris 1998). It would also contribute Na_2O and CaO, lowering both A/CNK and K_2O/Na_2O.

In their review on granite geochemistry Kemp and Hawkesworth (2003) called rocks formed under such conditions High-Sr leucogranites. The Glenelg River Complex, a muscovite-bearing High-Sr leucogranite in southeastern Australia, formed in a collisional setting where crustal anatexis of metasediments occurred at ~650-680 C° and 0.5-0.8 GPa (Kemp & Hawkesworth 2003).

The role of 022B is uncertain since no chemical analyzes is available from it. However, the presence of garnet and its biotite-rich mineralogy indicates that it may belong to the residue. Another possibility is that the garnet is peritectic and has been entrained in the migrating melt that 022B crystallized from. The presence of garnet would account for the HREE-depletion seen in 022D and 022E, even though other phases such as biotite, amphibole and zircon also partition HREE into the residue and could be called upon to explain the fractionation (Rollinson 1993; Kemp & Hawkesworth 2003).

In an experimental study by Patiño Douce and Harris (1998) were mica schist was melted under various P-T-H_2O conditions it was found that with a high H_2O-content (4 wt.%) at 700 C° and 1 GPa the following reaction occurred:

$$2Bt + 4Pl + 6Qtz \rightarrow 8\ Melt + 2Grt + 3Ms.$$

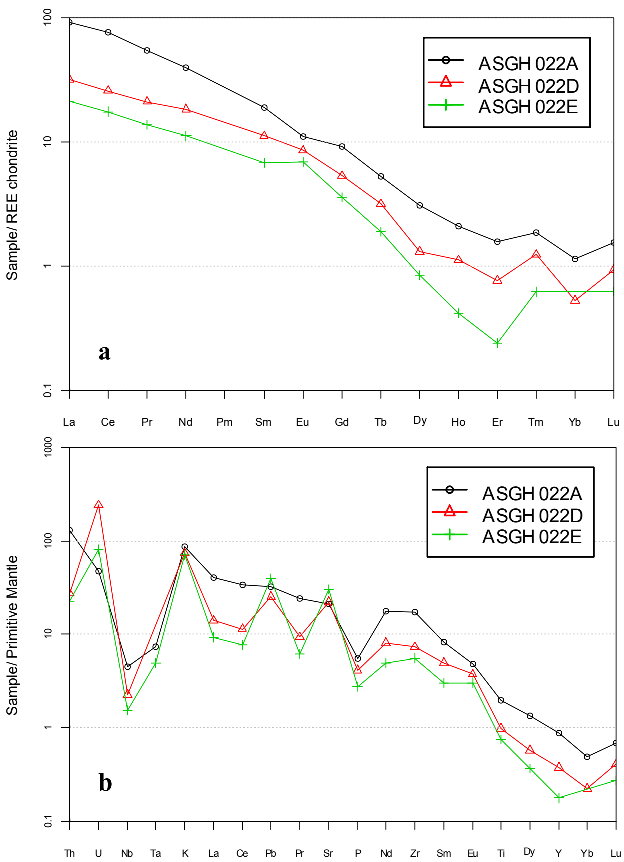

Fig. 22. Chondrite- (a) and primitive mantle (b) normalized curves of 022A, 022D and 022E.

Such a reaction could explain the presence of muscovite and garnet in 022B. However, it fails to explain why there is no muscovite in 022A. If both 022A and 022B are residues melting must have occurred through more then one reaction

Assuming that 022A was the main source of 022D and 022E other reactions involving both amphibole and biotite may be more suitable then the one given above. Since no thin section is available from 022A it has not been possible to identify peritectic minerals that may indicate what melting reactions took place.

The mafic nature of 022A may explain why it is richer in Ba compared to 022D and 022E. Plagioclase has high partition coefficients for Ba and the melts should therefore become enriched in it, as in the Glenelg River Complex (Kemp & Hawkesworth 2003). However, in mafic (andesitic) rocks amphibole, and in particular biotite, also have high partition coefficient for Ba (Rollinson 1993). The fact that 022A has such high Ba may therefore reflect that it primarily occur in its biotite and amphibole which remained largely refractory during melting.

The decreasing REE-content and increasing HREE-fractionation of 022D and 022E (fig. 22a) implies that 022E formed at a larger depth and later then 022D when their source was more depleted. Its more positive Eu/Eu* may be explained by changes in P-T-H_2O that would lead to increased melting of plagioclase, as was observed by Patiño Douce and Harris (1998) in mica schists. Thus, the granitoid likely constitutes several injections of magma of changing compositions.

022A have high Th/U whereas 022D and 022E shows low Th/U. The reasons for this are unclear. Zircon, a common mineral among the granitoids that contain both U and Th, is refractory (Kemp & Hawkesworth 2003). 022A show higher concentrations of Zr and Hf indicating that it has remained in the residue.

Doumbia *et al.* (1998) and Naba *et al.* (2004) investigated basin granitoids in the Ivory Coast and Burkina Faso, respectively. The geology in these areas is similar to Ghana, allowing for comparisons between the regions to be made. Doumbia *et al.* (1998) suggested that their biotite and biotite-muscovite granitoids were at least partly derived from melting of a source rock similar to their TTG-like belt granitoids. Naba *et al.* (2004) investigated a biotite-bearing basin granitoid that had intruded into a TTG-like belt granitoid and, like Doumbia *et al.* (1998), concluded that it was sourced from the belt granitoid. It is likely that the basin granitoids in this thesis are at least partly derived from a source containing belt granitoids, given their close association, both spatially and compositionally.

003A and 025A, also two-mica granitoids, display a similar behavior to 022D and 022E with positive Eu/Eu* and high Sr (fig. 23). This is also seen among 030A and 034A, which are biotite- and hornblende-bearing granitoids (fig. 23). It indicates that water-saturated melting does not necessarily need to end in a two-mica granitoid.

Rather, the variations in mineralogy between the leucosomes likely reflect differences in their sources. 030A and 034A occurs in the Kibi-Winneba belt and it is therefore likely that they also contain a component from mafic volcanics, such as basalt. Doumbia *et al.* (1998) suggested that one of their two-mica granitoids, which had a more mafic composition, could have partly been derived from a more mafic source, such as basalt from the greenstone belts. A more mafic source may explain why 030A and 034A have a biotite-hornblende assemblage rather than a two-mica.

003B, likely the corresponding residue to 003A, is similar to 022A in that it display a negative Eu/Eu*and lack a positive Sr-anomaly. Unlike 022A it is a two-mica granitoid. A two-mica mineral assemblage therefore cannot be considered as a characteristic of the leucosomes but must depend on other factors.

Two-mica granitoids occur in the central parts of the sedimentary basins; perhaps the two-mica granitoids contain a sedimentary component, not present in the biotite or biotite-hornblende granitoids? However, apart from the Sunyani and Cape Coast basin metasedimentary xenoliths are also present in 030A and 034A (Anders Scherstén, personal communication), showing that they were also affiliated with metasedimentary formations and my thus also contain a sedimentary component. Isotopic studies on Sr, Nd and O may provide insight into what sources, and to what degree, contributed to the basin granitoids.

The prevalence of biotite and biotite-hornblende granitoids in the Suhum basin and Kibi-Winneba belt, but lack of two-mica granitoids, which in turn occur in the northwestern basins, likely reflect the lack of sedi-

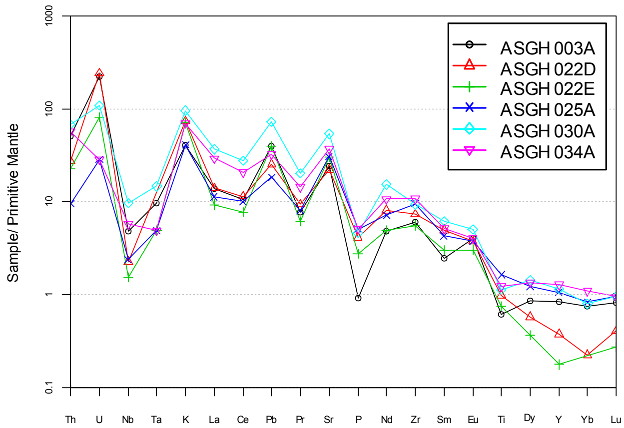

Fig. 23. High-Sr basin granitoids plotted against the primitive manlte of McDonough *et al.* (1992). Note the similar shape of their curves and the positive Sr-anomalies. The granitoids have both Bt-Ms and Bt-Hbl mineral assemblages.

ments in the Suhum basin (fig. 2).

Chemical characteristics, such as high Sr-Eu/Eu* or low Sr-Eu/Eu*, can be more useful in distinguishing leucogranites from their residue/source, instead of mineral assemblages. However, such a criteria need to be applied in a relative sense given that the Sr-content and Eu/Eu* of the granitoids sources varies.

With such a classification 003A, 022D, 022E and 028A would clearly qualify as high Sr-Eu/Eu* given that their corresponding residues displays lower values. No residue is available for 025A, 030A, 034A, 039A, PK 101 and PK 103. However, they have higher Sr and Eu/Eu* then their closest belt granitoids (019A, 032A and PK105) and, using these as a proxy for their source, they also qualify as high Sr-Eu/Eu* granitoids. 003B, 022A and 028B would correspond to low Sr-Eu/Eu* residues.

These relationships can be illustrated on Rb/Sr-Eu/Eu*, Sr/Nd-Rb/Ba and Eu/Eu*-Sr/Eu* diagrams (fig. 24). Kemp and Hawkesworth (2003) used these diagrams to discriminate between granitoids formed through melting in water-saturated and water-absent conditions (dehydration melting).

When plotting both belt and basin granitoids on a Rb/Sr-Eu/Eu* they form a trend of decreasing Rb/Sr with increasing Eu/Eu*. This is what can be expected in a water-saturated environment were melting of plagioclase occurs. Granitoids formed through dehydration melting in a water-absent environment instead show a vertical trend. This is a result of plagioclase being a largely refractory phase, sequestering Sr and Eu (Kemp & Hawkesworth 2003).

On a Sr/Nd-Rb/Ba diagram the granitoids have a near vertical trend. Increasing Sr/Nd among high Sr-Eu/Eu*granitoids relative to their residue or source is consistent with melting of plagioclase. The Rb/Ba varies, both increasing and decreasing among the high Sr-Eu/Eu*granitoids. Melting of plagioclase should lead to decreasing Rb/Ba relative to the source (Kemp & Hawkesworth 2003). However, as discussed above, increasing or unchanging ratios could reflect that Ba is partitioned into biotite and amphibole rather than plagioclase. Dehydration melting produces a trend towards higher Rb/Ba and lower Sr/Nd reflecting, again, that plagioclase remains a refractory phase (Kemp & Hawkesworth

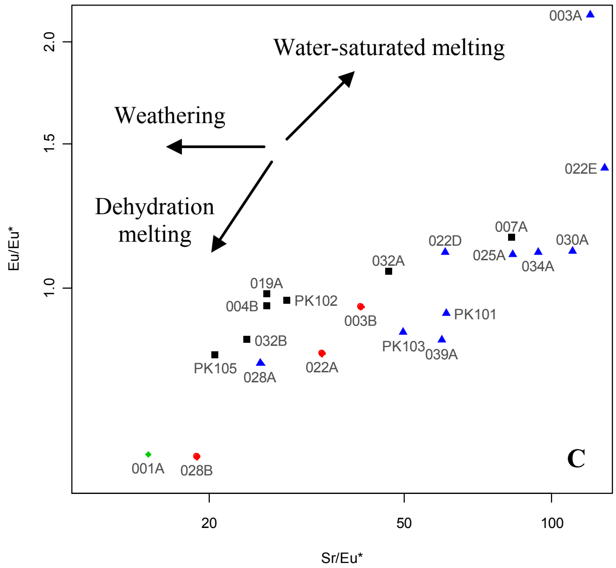

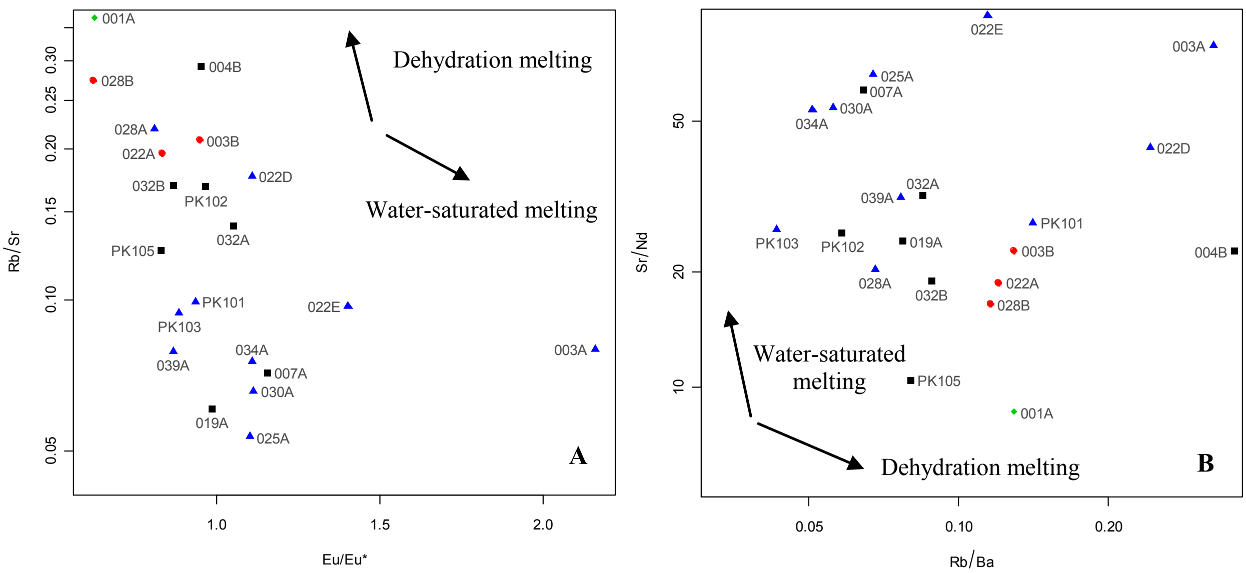

Fig. 24. Rb/Sr-Eu/Eu* (A), Sr/Nd-Rb/Ba (B) and Eu/Eu*-Sr/Eu* (C) diagrams showing the trends of dehydration and water-saturated melting. Blue triangles-high Sr-Eu/Eu* granitoids; black squares-belt granitoids; red circles-low Sr-Eu/Eu* granitoids; green circle- 001A. Note that 001A do not follow the trend of water-saturated melting seen among the high Sr-Eu/Eu*. Diagrams and trends from Kemp and Hawkesworth (2003).

2003).

Finally, in the Eu/Eu*-Sr/Eu* diagram granitoids formed from water-saturated and dehydration melting plot on the same igneous fractionation trend, but in opposite directions. This diagram plots the actual Sr and Eu concentrations as ratios against a extrapolated value for Eu ($\sqrt{(Sm*Gd)_N}$), i.e. the estimated value of Eu if no Eu-fractionation had occurred. Plagioclase controls the behavior of both Sr and Eu (in its reduced state). Fractionation would therefore move the granitoids towards lower values whereas melting of plagioclase would increase the Sr and Eu in the melt. On the Eu/Eu*-Sr/Eu* diagram the high Sr-Eu/Eu* granitoids follow the trend of water-saturated melting with increasing Sr and Eu/Eu* relative to their residue or source (Kemp & Hawkesworth 2003).

As mentioned previously, cumulates would follow the same trends as granitoids formed through partial melting in water-saturated conditions. The possibility that some of the granitoids are cumulates must therefore be taken into consideration.

The granitoids do not exhibit any obvious cumulatic textures. However, some of them do contain plagioclase phenocrysts that could have accumulated in the magma. To what degree such accumulation of plagioclase phenocrysts might have contributed to the granitoids Sr and Eu/Eu*-anomalies is hard to say.

In addition, since the chemical composition of most of their sources is not known, it is not possible to say with any certainty whether the granitoids composition is really the result of water-saturated melting.

In their study on belt and basin granitoids in the Ivory Coast Doumbia *et al.* (1998) suggested that peraluminous basin-type granitoids may have formed along transcurrent shear zones were water could infiltrate and induce melting. Heat could have been supplied either from underplating magmas or in a thermal corridor between two terranes of different thickness. Doumbia *et al.* (1998) estimated that anatexis had occurred between 600 -700 C° at 0.4-0.5 GPa. It is plausible that High-Sr leucogranites could result from such processes. Kemp and Hawkesworth (2003) noted that melting at the Glenelg River Complex appeared to have been initiated by influx of water from an external source, possibly from lower cooling magmas or dehydrating sediments.

Water-saturated melting together with a high geotherm would have made it possible for melting to occur, especially of mafic rocks, even though the Birimian terrane never reached high-grade metamorphic conditions (e.g. Eisenlohr and Hirdes 1992; this study).

Transcurrent deformation zones occur throughout southern Ghana (Feybesse *et al.* 2006). Such deformation zones extend from an upper brittle fault down into a ductile shear zone and may have acted as conduits for melts, explaining why many basin granitoids occur as elongate bodies in association with the faults (fig. 25). This has been reported from the Ivory Coast and Burkina Faso (Doumbia *et al.*1998; Naba *et al.* 2004). Shear heating in association with dehydrating metasediments may have provided the right conditions for melting.

However, ages of 003A (also applied to 003B), PK 101 (and presumably 039A, since its close proximity and similarity to PK 101 indicate they belong to the same granitoid) and PK 103 (Appendix C: table 1) show that they predate the transcurrent tectonic regime, as presented in the geodynamic model by Feybesse *et al.* (2006 – see section 3). Instead, they are associated with stage 1 of the Eburnean orogeny when the tectonic regime was compressional (Feybesse *et al.* 2006). However, Lompo (2010) argued that transcurrent shearing initiated at 2.13-2.11 Ga, based on ages of granitoids associated with such deformation zones. Determining the structural context of the basin granitoids in southern Ghana might bring more light to when transcurrent shearing initiated and whether basin granitoids were emplaced during both a compressional and transpressional regime.

7.2.1.4 Winneba granitoid

The Winneba granitoid (001A) is a biotite granite. However, its composition, together with its older Nd-model age (Taylor *et al.* 1992) and younger crystallization age sets it apart from the other granitoids.

001A have a large negative Eu/Eu* and, insofar, is similar to the low Sr-Eu/Eu* granitoids (see section 7.2.1.3). It could therefore be argued that 001A represent

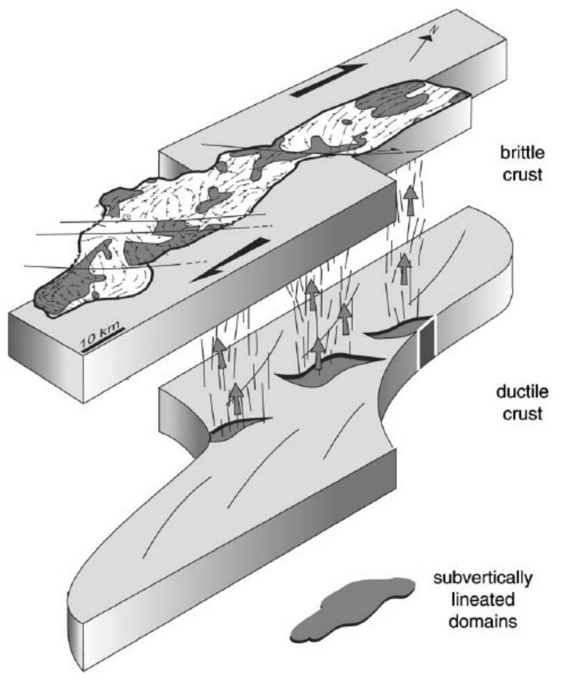

Fig. 25. Illustration of the emplacement of a basin granitoid from Burkina Faso in association with a transcurrent deformation zone. From Naba *et al.* (2004).

a residue from which a high Sr-Eu/Eu* granitoid has been extracted during melting in water-saturated conditions. However, since no such leucosome has been sampled the possibility that 001A itself is a high Sr-Eu/Eu*, extracted from a source with an even lower Eu/Eu*, also has to be considered. This would require a source with an even lower Eu/Eu* then 001A.

No belt granitoid from the southern Kibi-Winneba belt has been analyzed. 032A and PK 105, the closest belt granitoids, both have higher Sr and Eu/Eu* compared to 001A. If the source of 001A was anything like 032A or PK 105 it could not have formed through water-saturated melting. This leaves the possibility that 001A formed through dehydration melting and the breakdown of hydrous minerals such as biotite and amphibole.

On the diagrams in figure 24 the relationship between 032A and PK 105, as approximate sources, on one hand and 001A, as a leucogranite, on the other follows the trends for dehydration melting. This sets 001A apart from the other basin granitoids.

Dehydration melting occurs at higher temperatures (~700-750 C°) then water-saturated melting (Kemp & Hawkesworth 2003). As a result, dehydration melting would have occurred after water-saturated melting, during the later part of the Eburnean orogeny, perhaps in association with thermal relaxation. This would explain the younger age of 001A compared to the Cape Coast and Suhum basins. One question here is whether 030A and 034A also have the same age as 001A. Also, why is 001A the only granitoid that have formed through dehydration melting?

The high LREE and total REE of 001A is much larger then what is found in other granitoids. High total REE is observed in other basin granitoids, such as 022A (130.09 PPM), and may be the result of enrichment, due to their residual nature. However, the much larger total REE of 001A may at least partly reflect a fertile source. Such a source may well have been enriched Archean rocks which the isotopic composition of 001A indicates have formed a part of its source.

The high K_2O/Na_2O of 001A could also have been derived from such a fertile source. However, PK 103 also displays a relatively high K_2O/Na_2O. Since no Archean component has been reported in rocks apart from the Winneba granitoid the high ratio must depend on other factors, such as small degree partial melting.

Unusually high total REE among basin granitoids is also observed in 039A, PK 101 and PK 103. Given the lack of isotopic evidence for an Archean component outside of the Winneba granitoid (Taylor *et al.* 1992) these values cannot be attributed to an Archean component. Instead they likely reflect an inherited component from rocks similar to PK 105, which also have high total REE.

7.3 Eburnean orogeny: metamorphism, alteration and deformation

Epidote-group minerals, saussuritization and muscovite/sericite are common among the belt and basin granitoids. In addition, one basin granitoid – 022B – contains garnet. This indicates metamorphic conditions corresponding to greenschist-lower amphibolite facies. This is consistent with what has been reported for other belt granitoids in Ghana (e.g. Eisenlohr & Hirdes 1992; Doumbia *et al.* 1998; de Kock *et al.* 2011). Two leucocratic granitoids that intrude 004B display alteration bands containing phrenite (see Appendix A). These bands are not related to existing fractures but clearly postdate greenschist facies metamorphism of 004B. They thus correspond to a subsequent low-grade metamorphic overprint, perhaps in association with a fracture that has later healed. Phrenite has not been observed in any other belt or basin granitoid.

Foliation and dynamic recrystallization are common among both belt and basin granitoids, although the intensity varies. Foliation among the belt granitoids has been interpreted by other authors to be at least partly syn-intrusive (Eisenlohr & Hirdes 1992; Lompo 2010) while deformation and related recrystallization can been attributed to the Eburnian orogeny. Basin granitoids are syn- to postkinematic and foliation and deformation can therefore be attributed to the Eburnean orogeny (Eisenlohr & Hirdes 1992; Lompo 2010)

Both 007A and 019A have been extensively altered (Appendix A). The degree of alteration requires the presence of hydrothermal fluids. In Ghana, hydrothermal gold mineralizations are concentrated to the Ashanti and Sefwi belt (Leube *et al.* 1990). One hydrothermal gold mineralization from the Ashanti belt have been dated to 2063±9 Ma using hydrothermal xenotime related to the mineralization (Pigois *et al.* 2003). Given the documented presence of hydrothermal fluids it seems likely that the alteration found in 007A and 019A is associated with this ore-forming event and that the above age could also correspond to age of alteration. The fact that this type of extensive alteration has not been encountered in granitoids from other localities is a further indication that the alteration is associated with the hydrothermal gold mineralizations.

A carbonate phase (probably calcite or dolomite) occur as an accessory phase in many granitoids, both belt and basin types. The presence of carbonates within volcanic and sedimentary rocks have been attributed to percolating CO_2-rich fluids in association with hydrothermal gold mineralization (Feybesse *et al.* 2006 and references therein). It is therefore likely that the carbonates found in these granitoids are related to the same event. However, there is no geographical concentration of the occurrence of calcite nor is it found in 007A and 019A which, as discussed above, probably are related to the mineralization.

8 Conclusions

- The belt granitoids were emplaced in a subduction setting between 2232-2169 Ma. They show a trend of younging towards the northwest.

- The belt granitoids contain a slab melt component but also show variable mantle interaction. This is the result of a relatively steep angle of subduction which allows the slab melt to react with the mantle.

- Despite being sourced from slab melts the calc-alkaline behavior of the granitoids mean they do not qualify as true TTGs. They are rather an intermediate form between Archean and Post-Archean granitoids that reflects the change in granitoid genesis in subduction zones over time.

- PK 105 includes a sedimentary component and might represent a more evolved arc compared to the other belt granitoids. The presence of basin granitoids with high REE-concentrations and K_2O/Na_2O in the Suhum basin and Kibi-Winneba belt may indicate the extent of such an evolved arc.

- Basin granitoids were formed between 2134-2098 Ma and, like the belt granitoids, show a trend of younging towards the northwest. One notable exception is the Winneba granitoid which is younger then granitoids in both the Suhum and Cape Coast basins.

- The basin granitoids, with the exception of the Winneba granitoid, formed through water-saturated melting in which plagioclase was preferentially consumed whereas hydrous minerals were stabilized.

- Input from different sources, i.e. sediments or mafic volcanics, may explain the presence of both Bt-Ms and Bt-Hbl mineral assemblages among the basin granitoids.

- The Winneba granitoid formed through dehydration melting. This occurs at higher temperatures then water-saturated melting and may thus explain the younger age of the Winneba granitoid.

- Leucocratic granites occur as veins cross-cutting both basin and belt type granitoids. The age of 022C, 2 Ma younger then the basin granitoid 022A, indicate that the leucocratic granites were formed shortly after the basin granitoids.

- Metamorphism reached geenschist facies during the Eburnean orogeny. Deformation resulted in dynamic recrystallization.

- Two granitoids, 007A and 019A, from the Sefwi and Ashanti belts have been extensively altered by hydrothermal fluids. This alteration is possibly associated with hydrothermal gold mineralizations found in the same belts. Carbonate phases in the granitoids may also be related to these fluids.

9 Acknowledgements

I would like to thank my supervisor Anders Scherstén for providing me with the opportunity and material to work on these granitoids. I would also like to thank him for taking his time to answering questions, reading manuscripts and coming with suggestions that greatly imporved the thesis.

10 References

Abouchami, W., Boher, M., Michard, A. & Albarède, F., 1990: A major 2.1 Ga event of mafic magmatism in West Africa: an early stage of crustal accretion. *Journal of Geophysical Research 95*. 17.605 -17.629.

Adadey, K., Théveniaut, H., Clarke, B., Urien, P., Delor, C., Roig, R.J. & Feybesse, J.L., 2009: Geological Map Explanation, Map Sheet 0503B (1:100 000), CGS/BRGM/Geoman. Geological Survey Department of Ghana.

Attoh, K., Evans, M.J. & Bickford, M.E., 2006: Geochemistry of an ultramafic-rodingite rock association in the Paleoproterozoic Dixcove greenstone belt, southwestern Ghana. *Journal of African Earth Sciences 45*. 333-346.

Barker, F. & Arth, J.G., 1976: generation of trondhjemitic-tonalitic liquids and Archean bimodal trondhjemite-basalt suites. *Geology 4*. 596-600.

Boher, M., Abouchami, W., Michard, A., Albarède, F. & Arndt, N.T., 1992: Crustal growth in West Africa at 2.1 Ga. *Journal of Geophysical Research 97*. 345-369.

Boynton, W.V., 1984: Geochemistry of the rare earth elements: meteorite studies. In: Henderson, P. (ed.), *Rare earth element geochemistry*. Elsevier, pp. 63-114.

Chalokwu, C.I., Ghazi, M.A. & Foord, E.E., 1997: Geochemical characteristics and K-Ar ages of rare-metal bearing pegmatites from the Birimian of southeastern Ghana. *Journal of African Earth Sciences 24*. 1-9.

Condie, K.C., 2005: TTGs and adakites: Are they both slab melts?. *Lithos 80.* 33-44.

Dampare, S.B., Shibata, T., Asiedu, D.K., Osae, S. & Banoeng-Yakubo, B., 2008: Geochemistry of Paleoproterozoic metavolcanic rocks from the southern Ashanti volcanic belt, Ghana: Petrogenetic and tectonic setting implications. *Precambrian Research 162.* 403-423.

Davies, D.W., Hirdes, W., Schaltegger, U. & Nunoo, E.A., 1994: U-Pb age constraint on deposition and provenance of Birimian gold-bearing Tarkwaian sediments in Ghana, West Africa. *Precambrian Research 67*. 89-107.

Defant, M.J. & Drummond, M.S., 1990: Derivation of some modern arc magmas by melting of young subducted lithosphere. *Nature 347*. 662-665.

de Kock, G.S., Armstrong, R.A., Siegfried, H.P. & Thomas, E., 2011: Geochronology of the Birim Supergroup of the West African craton in the Wa-Bolé region of west-central Ghana: Implications for the stratigraphic framework. *Journal of African earth Sciences 59*. 1-40.

Doumbia, S., Pouclet, A., Kouamelan, A., Peucat, J.J., Vidal, M. & Delor, C., 1998. Petrogenesis of juvenile-type Birimian (Paleoproterozoic) granitoids in central Côte d'Ivoire, West Africa: geochemistry and geochronology. *Precambrian Research 87*. 33-63.

Eisenlohr, B.N., & Hirdes, W., 1992: The structural development of the early Proterozoic Birimian and Tarkwaian rocks of southwest Ghana, West Africa. *Journal of African Earth Sciences 14.* 313-325

Feybesse, J.-L., Billa, M., Guerrot, C., Duguey, E., Lescuyer, J.-L., Milesi, J.,.P. & Bouchot, V., 2006: The Paleoproterozoic Ghanian province: geodynamic model and ore controls, including regional stress modeling. *Precambrian Research 149*. 149 -196.

Foley, S., Tiepolo, M. & Vannucci, R., 2002: Growth of early continental crust controlled by melting of amphibolite in subduction zones. *Nature 417*. 837 -840.

Hawkesworth, C., Turner, S., Peate, D., McDermott, F. & van Calsteren, P., 1997: Elemental U and Th variations in island arc rocks: implications for U-series isotopes. *Chemical Geology 139.* 207-221.

Hirdes, W., Davis, D.W. & Eisenlohr, B.N., 1992: Reassessment of Proterozoic granitoid ages in Ghana on the basis of U/Pb zircon and monazite dating. *Precambrian Research 56.* 89-96.

Hirdes, W., Senger, R., Adjej, J., Efa, E., Loh, G.W. & Tettey, A., 1993: Explanatory notes for the Geological Map of southwest Ghana, 1:100 000: Sheets Wiawso (0603D), Asafo (0603C), Kukuom (0603B), Goasso (0603A), Sunyani (0703D) and Berekum (0703C). Geologische Jahrbuch B83. Schwezerbartsche Verlagsbuchhandlung, Stuttgart, 139 pp.

Hirdes, W., Davis, D.W., Lüdtke, G. & Konan, G., 1996: Two generations of Birimian (Paleoproterozoic) volcanic belts in northeastern Côte d'Ivoire (West Africa): consequences for the 'Birimian controversy'. *Precambrian Research 80*. 173-191.

Hirdes, W. & Davis, D.W., 1998: First U-Pb zircon age of extrusive volcanism in the Birimian supergroup of Ghana/West Africa. *Journal of African Earth Sciences 27*. 291-294.

Hirdes, W. & Davis, D.W,, 2002: U-Pb geochronology of Paleoproterozoic rocks in the southern part of the Kedougou-Kéniéba inlier, Senegal, West Africa: Evidence for diachronous accretionary development of the Eburnean province. *Precambrian Research 118*. 83-99.

Janoušek, V., Farrow, C. M. & Erban, V., 2006: Interpretation of whole-rock geochemical data in igneous geochemistry: introducing Geochemical Data Toolkit (GCDkit). *Journal of Petrology 47(6)*. 1255-1259

John, T., Klemd, R., Hirdes, W. & Loh, G., 1999: The metamorphic evolution of the Paleoproterozoic (Birimain) volcanic Ashanti belt (Ghana, West Africa). *Precambrian Research 98.* 11-30.

Kemp, A.I.S. & Hawkesworth, C.J., 2003: Granitic perspectives on the generation and secular evolution of the continental crust. In R.L.Rudnick (ed.): Treatise on Geochemistry, 349-410. Elsevier Ltd.

Leube, A., Hirdes, W., Mauer, R. & Kesse, G.O., 1990: The early Proterozoic Birimian super group of Ghana and some aspects of its associated gold mineralization. *Precambrian Research 46*. 139-165.

Loh, G. & Hirdes, W., 1996: Explanatory notes for the Geological Map of southwest Ghana, 1:100 000: Sheets Sekondi (0402A) and Axim (0403B): Ghana Geological Survey Bulletin 49. 63 pp.

Lompo, M., 2010: Paleoproterozoic structural evolution of the Man-Leo shield (West Africa). Key structures for vertical to transcurrent tectonics. *Journal of African Earth Sciences 58.* 19-36.

Martin, H., 1987: Archean and modern granitoids as indicators of changes in geodynamic processes. *Revista Brasileira de Geociências 17*. 360-365.

Martin, H., 1993: The mechanisms of petrogenesis of the Archean continental crust – comparison with modern processes. *Lithos 30.* 373-388.

Martin, H. & Moyen, J-F., 2002: Secular changes in tonalite-trondhjemite-granodiorite composition as markers of the progressive cooling of Earth. *Geology 30.* 319-322.

Martin, H., Smithies, R.H., Rapp, R., Moyen, J-F. & Champion, D., 2005: An overview of adakite, tonalite-trondhjemite-granodiorite (TTG), and sanukitoid: Relationships and some implications for crustal evolution. *Lithos 79.* 1-24.

McDonough, W.F., Sun, S-S., Ringwood, A.E., Jagoutz, E., & Hofmann, A.W., 1992: Potassium, rubidium and cesium in the earth and moon and the evolution of the mantle of the earth. *Geochimica et Cosmochimica Acta 56.* 1001-1012.

Naba, S., Lompo, M., Debat, P., Bouchez, J.L. & Béziet, D., 2004: Structure and emplacement model for late-orogenic Paleoproterozoic granitoids: the Tenkodogo-Yamba elongate pluton. *Journal of African Earth Sciences 38*. 41-57.

Oberthür, T., Vetter, U., Davis, D.W. & Amanor, J.A., 1998: Age constraints on gold mineralization and Paleoproterozoic crustal evolution in the Ashanti belt of southern Ghana. *Precambrian Research 89.* 129-143.

Patiño Douce, A.E. & Harris, N., 1998: Experimental constraints on Himalayan anatexis. *Journal of Petrology 39*. 689-710.

Pearce, J.A., Harris, N.B.W. & Tindle, A.G., 1984: Trace element discrimination diagrams for the tectonic interpretation of granitic rocks. *Journal of Petrology 25*. 956-983.

Pigois. J-P., Groves, D.I., Fletcher, I.R., McNaughton, N.J. & Snee, L.W., 2003: Age constraints on Tarkwaian paleoplacer and lode-gold formation in the Tarkwa-Damang district, SW Ghana. *Mineralium Deposita 38.* 695-714.

Rollinson, H., 1993: Using geochemical data: Evaluation, Presentation Interpretation. Longman Group Ltd. 352 pp.

Sylvester, P.J. & Attoh, K., 1992: Litostratigraphy and composition of 2.1 Ga greenstone belts of the West African Craton and their bearing on crustal evolution and the Archean-Proterozoic boundary. *Journal of Geology 100.* 377-392.

Sun, S.S. & McDonough, W.F., 1989: Chemical and isotopic systematics of oceanic basalts: implications for mantle composition and processes. In Saunders, A.D. and Norry, M.J. (eds): Magmatism in ocean basins. Geological Society of London special publication 42. 313-345.

Tarney, J. & Jones, C.E., 1994: Trace element geochemistry of orogenic igneous rocks and crustal growth models. *Journal of the Geological Society (London) 151*. 855-868.

Taylor, P.N., Moorbath, S., Leube, A. & Hirdes, W., 1992: Early Proterozoic crustal evolution in the Birimian of Ghana: constraints from geochronology and isotope geochemistry. *Precambrian Research 56*. 97-111
.

Zitsmann, A., Kiessling, R. & Loh, G., 1997: Geology in the Bui belt area in Ghana. In Zitsmann, A. (ed.): Geological, geophysical and geochemical investigations in the Bui belt area in Ghana. Geologische Jahrbuch, Reihe B 88. 7-112.

grained biotite. Accessory phases are fine grained epidote and clinozoisite, zircon, a carbonate phase – probably calcite or dolomite, apatite and opaques. On the basis of the estimated relative abundance of plagioclase, K-feldspar and quartz the sample is interpreted as granite. The mafic content of the sample is low and it is thus considered to be leucocratic.

Plagioclase grains exhibit albite twinning and a small degree of saussuritization. K-feldspar exhibits tartan twinning and a small degree of sericitization. Quartz display subgrains. Plagioclase, K-feldspar and quartz display bulging grain boundaries and nucleation. Biotite grains are brown and define a foliation. Epidote and clinozoisite are often found in association with biotite. A band of fine grained phrenite, muscovite, a carbonate phase and saussuritization cuts the sample and is not connected to existing fractures. The sample can be divided into two domains, one coarser plagioclase-rich and another with more fine grained crystals richer in K-feldspar.

004B - Bt-Hbl tonalite

Major phases are fine to medium grained plagioclase, quartz, biotite and hornblende. Minor phases are fine to medium grained epidote, clinozoisite and an unidentified, high relief, isotropic mineral – possibly retrogressed garnet or spinel. Accessory phases are titanite, apatite, zircon and opaques. On the basis of the estimated relati-

Appendix A

Geochemical data for the granitoids. Radiometric ages and eNd_t by Anders Scherstén (unpublished data). Map units are taken from the geological map (1:100000) published by thr Geological Survey Department (GSD) in Accra, Ghana (reference unknown). Total iron is given as Fe_2O_3 . REE has been normalized (N) to chondrite values by Boynton (1984).

Sample			ASGH 001A	ASGH 003A	ASGH 003B	ASGH 022A	ASGH 022D	ASGH 022E	ASGH 025A	ASGH 028A	ASGH 028B	ASGH 030A
Rock type			Bt granite	Bt-Ms granodiorite	Bt-Ms granodiorite	Bt-Hbl granitoid	Bt-Ms tonalite	Bt-Ms tonalite	Bt±Ms granitoid	Bt-Hbl granite	Bt-Hbl granite	Bt-Hbl granite
Map unit			gsa	gsb	gsb	gsb	gsb	gsb	gsb	tmmg	tmmg	gsb
Location			Kibi-Winneba	Cape Coast	Cape Coast	Sunyani	Sunyani	Sunyani	Kumasi	Suhum	Suhum	Kibi-Winneba
Granite type			Basin type	Basin type	Basin type	Basin type	Basin type	Basin type	Basin type	Basin type	Basin type	Basin type
Age(Ma)			2090	2124		2094						
εNd_t				1.50			1.40	1.70	1.10			
wt %		MDL										
	SiO2	0.01	66.81	72.27	67.90	72.56	68.80	72.65	70.93	67.42	63.93	69.35
	Al2O3	0.01	15.88	15.95	16.79	15.12	17.95	15.47	14.47	15.52	15.43	15.78
	Fe2O3	0.04	3.45	1.02	2.36	1.75	1.45	0.84	2.99	3.94	5.82	2.05
	MgO	0.01	1.08	0.31	0.78	0.53	0.61	0.49	1.23	0.88	1.57	0.75
	CaO	0.01	2.58	2.88	2.60	1.59	1.87	1.71	2.80	2.90	3.51	2.47
	Na2O	0.01	3.58	5.38	4.88	3.65	5.62	5.35	4.94	4.39	4.30	5.24
	K2O	0.01	3.93	1.18	3.01	2.51	2.13	2.07	1.18	3.27	3.11	2.78
	TiO2	0.01	0.57	0.13	0.33	0.42	0.21	0.16	0.35	0.43	0.71	0.24
	P2O5	0.01	0.17	0.02	0.12	0.12	0.09	0.06	0.11	0.10	0.17	0.10
	MnO	0.01	0.03	0.02	0.02	0.02	0.01		0.03	0.05	0.08	0.03
	Cr2O3	0.002		0.002	0.020				0.003		0.004	0.002
	LOI	-5.1	1.50	0.70	1.00	1.50	1.10	1.00	0.70	0.80	1.10	0.80
	Sum	0.01	99.62	99.84	99.77	99.77	99.85	99.75	99.74	99.73	99.74	99.60
ppm		MDL										
	Ni	20										21
	Sc	1	5	3	4	2	2	2	5	7	10	4
	Ba	1	1270	126	746	735	341	539	514	1190	878	1340
	Co	0.2	102.1	94.9	57.9	65.5	54.2	113.5	100.7	69.1	76.5	101.3
	Cs	0.1	5.1	1.7	2.1	1.6	2.9	1.4	8.5	1.7	3.2	3.3
	Ga	0.5	19.5	16.8	20.5	20.5	26.4	20.8	21.1	17.6	18.8	16.4
	Hf	0.1	7.1	2.4	4.5	5.6	2.4	2.0	2.7	5.6	5.1	3.1
	Nb	0.1	13.0	3.4	5.6	3.2	1.6	1.1	1.7	6.2	10.6	6.9
	Rb	0.1	163.7	41.0	96.5	88.4	82.8	61.7	34.6	81.0	101.8	74.8
	Sr	0.5	446.8	512.4	462.8	450.3	467.9	634.6	647.6	367.7	370.4	1133.8
	Ta	0.1	1.3	0.4	0.3	0.3		0.2	0.2	0.4	0.5	0.6
	Th	0.2	41.2	4.3	12.8	10.9	2.3	1.9	0.8	5.6	5.0	5.7
	U	0.1	2.5	4.7	1.5	1.0	5.1	1.7	0.6	0.5	0.5	2.3
	V	8	54		41	27	25	19	52	25	47	28
	Zr	0.1	248.2	67.4	159.6	195.0	82.0	62.3	106.1	184.6	177.2	104.6
	Y	0.1	14.2	3.8	5.2	4.0	1.7	0.8	4.8	15.8	26.0	5.2
	La	0.1	79.1	9.8	29.4	28.8	9.9	6.6	8.0	26.5	26.3	26.0
	Ce	0.1	153.0	19.2	57.8	61.6	20.9	14.2	18.4	51.7	55.6	51.0
	Pr	0.02	15.73	2.14	5.98	6.73	2.58	1.69	2.23	5.20	6.12	5.55
	Nd	0.3	52.0	6.5	20.3	24.0	11.0	6.7	9.8	18.0	22.5	20.9
	Sm	0.05	7.85	1.08	3.07	3.68	2.19	1.33	1.90	3.29	4.45	2.72
	Eu	0.02	1.37	0.68	0.79	0.81	0.63	0.51	0.63	0.86	0.90	0.84
	Gd	0.05	5.69	0.86	2.11	2.40	1.38	0.93	1.61	3.20	4.38	1.96
	Tb	0.01	0.68	0.12	0.27	0.25	0.15	0.09	0.21	0.50	0.72	0.23
	Dy	0.05	3.00	0.63	1.07	0.99	0.42	0.27	0.90	2.86	4.13	1.05
	Ho	0.02	0.49	0.12	0.19	0.15	0.08	0.03	0.18	0.56	0.90	0.17
	Er	0.03	1.22	0.40	0.51	0.33	0.16	0.05	0.44	1.58	2.51	0.43
	Tm	0.01	0.16	0.05	0.09	0.06	0.04	0.02	0.07	0.21	0.34	0.06
	Yb	0.05	0.90	0.37	0.48	0.24	0.11		0.41	1.48	2.39	0.39
	Lu	0.01	0.16	0.06	0.10	0.05	0.03	0.02	0.07	0.21	0.36	0.07
	LaN		255.16	31.61	94.84	92.90	31.94	21.29	25.81	85.48	84.84	83.87
	CeN		189.36	23.76	71.53	76.24	25.87	17.57	22.77	63.99	68.81	63.12
	PrN		128.93	17.54	49.02	55.16	21.15	13.85	18.28	42.62	50.16	45.49
	NdN		86.67	10.83	33.83	40.00	18.33	11.17	16.33	30.00	37.50	34.83
	SmN		40.26	5.54	15.74	18.87	11.23	6.82	9.74	16.87	22.82	13.95
	EuN		18.64	9.25	10.75	11.02	8.57	6.94	8.57	11.70	12.24	11.43
	GdN		21.97	3.32	8.15	9.27	5.33	3.59	6.22	12.36	16.91	7.57
	TbN		14.35	2.53	5.70	5.27	3.16	1.90	4.43	10.55	15.19	4.85
	DyN		9.32	1.96	3.32	3.07	1.30	0.84	2.80	8.88	12.83	3.26
	HoN		6.82	1.67	2.65	2.09	1.11	0.42	2.51	7.80	12.53	2.37
	ErN		5.81	1.90	2.43	1.57	0.76	0.24	2.10	7.52	11.95	2.05
	TmN		4.94	1.54	2.78	1.85	1.23	0.62	2.16	6.48	10.49	1.85
	YbN		4.31	1.77	2.30	1.15	0.53		1.96	7.08	11.44	1.87
	LuN		4.97	1.86	3.11	1.55	0.93	0.62	2.17	6.52	11.18	2.17

Appendix A cont.

Sample		ASGH 034A	ASGH 039A	PK101	PK103	ASGH 004B	ASGH 007A	ASGH 019A	ASGH 032A	ASGH 032B	PK102	PK105
Rock type		Bt-Hbl granite	Bt granitoid	Bt-Hbl tonalite	Bt-Hbl granite	Bt-Hbl tonalite	Bt-Hbl tonalite	Bt-Hbl tonalite	Bt-Hbl granodiorite	mafic enclave	Bt-Hbl granodiorite	Bt-Hbl granodiorite
Map unit		gsb	tmmg	tmmg	gsbg	gvh	gvh	gvh	gsb	gsb	tmmg	tmmg
Location		Kibi-Winneba	Suhum	Suhum	Suhum	Cape Coast	Ashanti	Sefwi	Kibi-Winneba	Kibi-Winneba	Suhum	Suhum
Granite type		Basin type	Basin type	Basin type	Basin type	Belt type	Belt type	Belt type	Belt type	Belt type	Belt type	Belt type
Age(Ma)				2130	2134		2172	2169			2180	2232
εNd_t										1.70		1.70
wt %	MDL											
SiO2	0.01	69.43	67.08	63.95	66.07	61.21	66.54	56.45	67.93	60.22	67.55	70.34
Al2O3	0.01	15.61	16.03	17.06	15.01	15.62	15.75	17.03	15.46	16.58	15.04	14.53
Fe2O3	0.04	2.38	3.53	4.44	4.26	6.37	3.45	8.04	2.89	4.99	3.76	3.22
MgO	0.01	0.95	1.34	1.76	1.88	3.78	1.58	2.96	1.39	2.48	1.41	0.93
CaO	0.01	2.89	3.33	3.74	3.41	4.86	3.73	7.20	2.89	4.28	3.89	3.81
Na2O	0.01	5.11	4.46	4.84	3.74	3.49	4.48	3.61	4.72	4.93	4.06	4.06
K2O	0.01	2.02	2.08	1.94	3.45	2.22	1.94	0.83	2.56	3.10	2.23	1.35
TiO2	0.01	0.26	0.40	0.58	0.42	0.65	0.32	0.86	0.37	0.58	0.41	0.30
P2O5	0.01	0.11	0.16	0.23	0.16	0.22	0.10	0.19	0.13	0.36	0.09	0.09
MnO	0.01	0.04	0.04	0.04	0.07	0.13	0.07	0.11	0.05	0.08	0.06	0.04
Cr2O3	0.002	0.006	0.006	0.003			0.004		0.004	0.008	0.004	
LOI	-5.1	0.90	1.20	1.20	1.10	1.20	1.80	2.50	1.30	2.10	1.20	1.20
Sum	0.01	99.68	99.70	99.75	99.59	99.77	99.76	99.79	99.71	99.68	99.71	99.82
ppm	MDL											
Ni	20					49				25	24	
Sc	1	4	4	3	10	16	8	22	6	11	9	6
Ba	1	1163	879	495	1642	378	739	276	893	1074	1021	381
Co	0.2	78.7	53.6	49.4	78.4	52.2	49.6	61.4	104.7	58.1	99.9	66.4
Cs	0.1	2.9	0.5	0.6	0.6	11.8	1.0	0.3	2.5	5.6	1.5	0.2
Ga	0.5	17.9	17.9	18.5	15.4	16.8	17.8	17.1	20.3	22.7	14.6	14.8
Hf	0.1	3.3	3.7	6.0	3.8	3.3	2.9	2.7	3.6	4.0	4.1	5.4
Nb	0.1	4.1	4.2	5.3	3.9	5.7	2.4	4.2	3.8	10.4	6.1	2.8
Rb	0.1	59.1	67.3	69.9	70.6	135.9	47.4	21.3	75.5	94.9	59.4	30.5
Sr	0.5	783.0	851.3	702.1	748.3	463.2	660.6	350.4	536.3	559.4	352.6	242.2
Ta	0.1	0.2	0.3	0.2	0.2	0.3	0.1	0.2	0.3	0.8	0.6	0.2
Th	0.2	4.8	13.4	11.9	19.6	2.0	2.3	1.8	4.1	4.3	3.7	21.8
U	0.1	0.6	0.5	0.4	0.3	1.1	1.6	0.5	1.6	3.8	1.1	0.4
V	8	33	39	55	67	126	61	146	46	91	52	43
Zr	0.1	120.4	145.3	218.5	145.9	137.3	89.4	77.9	111.1	139.9	128.3	207.2
Y	0.1	5.8	5.6	4.7	9.6	18.3	8.4	17.2	7.1	15.5	13.4	8.1
La	0.1	20.8	44.4	51.2	44.9	19.2	11.8	13.2	19.0	22.8	15.7	43.1
Ce	0.1	38.0	83.3	92.9	87.7	44.1	24.3	28.0	40.1	54.3	32.8	81.9
Pr	0.02	3.99	8.37	8.55	8.61	5.28	2.80	3.45	4.62	6.97	3.75	7.43
Nd	0.3	14.6	27.1	26.0	28.9	20.4	11.0	14.5	16.8	29.5	13.9	23.3
Sm	0.05	2.27	3.78	3.00	3.91	4.03	1.87	2.92	2.95	5.94	2.80	2.90
Eu	0.02	0.68	0.91	0.79	0.98	1.24	0.68	0.97	0.89	1.49	0.87	0.72
Gd	0.05	1.55	2.73	2.23	2.94	3.93	1.73	3.10	2.28	4.66	2.70	2.42
Tb	0.01	0.21	0.29	0.21	0.38	0.57	0.25	0.50	0.28	0.61	0.43	0.28
Dy	0.05	0.99	1.34	0.94	1.79	3.18	1.37	3.00	1.29	2.93	2.43	1.43
Ho	0.02	0.20	0.20	0.16	0.33	0.63	0.26	0.59	0.23	0.49	0.46	0.27
Er	0.03	0.54	0.46	0.41	0.91	1.85	0.70	1.67	0.61	1.39	1.32	0.77
Tm	0.01	0.08	0.05	0.05	0.11	0.27	0.10	0.24	0.07	0.17	0.17	0.09
Yb	0.05	0.54	0.37	0.42	0.83	1.81	0.71	1.55	0.56	1.22	1.27	0.76
Lu	0.01	0.07	0.05	0.05	0.12	0.31	0.11	0.24	0.08	0.18	0.19	0.12
LaN		67.10	143.23	165.16	144.84	61.94	38.06	42.58	61.29	73.55	50.65	139.03
CeN		47.03	103.09	114.98	108.54	54.58	30.07	34.65	49.63	67.20	40.59	101.36
PrN		32.70	68.61	70.08	70.57	43.28	22.95	28.28	37.87	57.13	30.74	60.90
NdN		24.33	45.17	43.33	48.17	34.00	18.33	24.17	28.00	49.17	23.17	38.83
SmN		11.64	19.38	15.38	20.05	20.67	9.59	14.97	15.13	30.46	14.36	14.87
EuN		9.25	12.38	10.75	13.33	16.87	9.25	13.20	12.11	20.27	11.84	9.80
GdN		5.98	10.54	8.61	11.35	15.17	6.68	11.97	8.80	17.99	10.42	9.34
TbN		4.43	6.12	4.43	8.02	12.03	5.27	10.55	5.91	12.87	9.07	5.91
DyN		3.07	4.16	2.92	5.56	9.88	4.25	9.32	4.01	9.10	7.55	4.44
HoN		2.79	2.79	2.23	4.60	8.77	3.62	8.22	3.20	6.82	6.41	3.76
ErN		2.57	2.19	1.95	4.33	8.81	3.33	7.95	2.90	6.62	6.29	3.67
TmN		2.47	1.54	1.54	3.40	8.33	3.09	7.41	2.16	5.25	5.25	2.78
YbN		2.58	1.77	2.01	3.97	8.66	3.40	7.42	2.68	5.84	6.08	3.64
LuN		2.17	1.55	1.55	3.73	9.63	3.42	7.45	2.48	5.59	5.90	3.73

Appendix B

Table 1. Selected data on belt granitoids

Sample	A/CNK	Rock type	$(La/Yb)_N$	$(Gd/Yb)_N$	Yb_N	Tot. REE	Eu/Eu*	$(Nb/La)_{PM}$	$(Ce/Pb)_{PM}$	$(Th/U)_{PM}$	K_2O/Na_2O	#Mg
ASGH 004B	0,92	Bt-Hbl tonalite	7,15	1,75	9	106,80	0,95	0,29	1,55	0,45	0,64	70
ASGH 007A	0,97	Bt-Hbl tonalite	11,20	1,97	3	57,68	1,16	0,2	0,25	0,36	0,43	64
ASGH 019A	0,85	Bt-Hbl tonalite	5,74	1,61	7	73,93	0,99	0,32	0,57	0,9	0,23	59
ASGH 032A	0,98	Bt-Hbl granodiorite	22,87	3,29	3	89,76	1,05	0,2	0,24	0,64	0,54	66
ASGH 032B	0,86	Bt granodiorite	12,60	3,08	6	132,65	0,87	0,45	0,27	0,28	0,63	66
PK102	0,93	Bt-Hbl granodiorite	8,33	1,72	6	78,79	0,97	0,39	0,44	0,84	0,55	60
PK105	0,96	Bt-Hbl granodiorite	38,23	2,57	4	165,49	0,83	0,06	0,62	13,63	0,33	53

Table. 2. Selected data on basin granitoids

Sample	A/CNK	Rock type	$(La/Yb)_N$	$(Gd/Yb)_N$	Yb_N	Tot. REE	Eu/Eu*	$(Nb/La)_{PM}$	$(Ce/Pb)_{PM}$	$(Th/U)_{PM}$	K_2O/Na_2O	#Mg
ASGH 001A	1,07	Bt granite	59,25	5,10	4	321,35	0,63	0,16	0,53	4,12	1,10	55
ASGH 003A	1,04	Bt-Ms granodiorite	17,86	1,88	2	42,01	2,16	0,34	0,27	0,23	0,22	55
ASGH 003B	1,05	Bt-Ms granodiorite	41,29	3,55	2	122,16	0,95	0,19	0,45	2,13	0,62	57
ASGH 022A	1,30	Bt-Hbl granitoid	80,90	8,07	1	130,09	0,83	0,11	1,04	2,73	0,69	55
ASGH 022D	1,20	Bt-Ms tonalite	60,68	10,12	1	49,57	1,11	0,16	0,45	0,11	0,38	63
ASGH 022E	1,09	Bt-Ms tonalite	-	-	-	32,44	1,40	0,17	0,2	0,28	0,39	70
ASGH 025A	1,00	Bt±Ms granitoid	13,15	3,17	2	44,85	1,10	0,21	0,55	0,33	0,24	62
ASGH 028A	0,97	Bt-Hbl granite	12,07	1,75	7	116,15	0,81	0,23	0,63	2,8	0,74	47
ASGH 028B	0,92	Bt-Hbl granite	7,42	1,48	11	131,60	0,62	0,4	0,77	2,5	0,72	52
ASGH 030A	0,98	Bt-Hbl granite	44,95	4,06	2	111,37	1,11	0,26	0,38	0,62	0,53	59
ASGH 034A	0,99	Bt-Hbl granite	25,97	2,32	3	84,52	1,11	0,2	0,64	2	0,40	61
ASGH 039A	1,02	Bt granitoid	80,90	5,95	2	173,35	0,87	0,09	1,04	6,7	0,47	60
PK101	1,01	Bt-Hbl tonalite	82,19	4,29	2	186,91	0,93	0,1	1,71	7,44	0,40	61
PK103	0,93	Bt-Hbl granite	36,47	2,86	4	182,41	0,88	0,09	0,6	16,33	0,92	64

Appendix C

Table. 1. Unpublished radiometric ages by Dr. Anders Scherstén. Sample locations are displayed in figure 2.

Sample	Location	Rock type	Age (Ga) ±2σ	Comment
ASGH 001A	Kibi-Winneba belt	Bt-granite	2,090±0,060	U-Pb zircon
ASGH 003A	Cape Coast basin	Bt-Ms granodiorite	2,124±0,006	U-Pb zircon
ASGH 007	Ashanti belt	Bt-Hbl tonalite	2,172±0,012	U-Pb zircon
ASGH 019	Sefwi belt	Bt-Hbl tonalite	2,169±0,013	U-Pb zircon
ASGH 022A	Sunyani basin	Bt-Hbl granitoid	2,094±0,004	U-Pb zircon
ASGH 022C	Sunyani basin	Leucocratic granite	2,092±0,004	U-Pb zircon
PK 101	Suhum basin	Bt-Hbl tonalite	2,130±0,010	U-Pb zircon
PK 102	Suhum basin	Bt-Hbl granite	2,180±0,004	U-Pb zircon
PK 103	Suhum basin	Bt-Hbl granodiorite	2,134±0,010	U-Pb zircon
PK 105	Suhum basin	Bt-Hbl granodiorite	2,232±0,005	U-Pb zircon

Table. 2. Published radiometric ages from the Birimian terrane in southern Ghana. When it has not been possible to verify the source of an age it is referred to the geological map of Ghana (1:1000000) published by the Geological Survey Department (GSD) in Accra, Ghana (reference unknown). In such cases a nearby town or lake is given as a geographical reference and the rock type is given from the legend of the geological map (e.g. bmb, tmmg). Data from Hirdes *et al.* (1993), Loh and Hirdes (1996), Zitsmann *et al.* (1997) and Adadey *et al.* (2009) has been taken from de Kock *et al.* (2011).

Sample/Location	Rock type	Age (Ga) ±2σ	Comment	Reference
Suhum basin				
Lake Weija	gsbg	2,106±0,001	U-Pb zircon	Geological map
Kwanyako	tmmg	2,132±0,004	U-Pb zircon	Geological map
G1d	monzonite	2,158±0,005	Pb-Pb zircon	Feybesse *et al.* (2006)
Senya Bereku	bmb	2,165±0,009	U-Pb zircon	Geological map
Kibi-Winneba belt				
Winneba	gsa	2,113±0,001	U-Pb zircon	Geological map
G113B	granodiorite	2,200±0,004	Pb-Pb zircon	Feybesse *et al.* (2006)
Cape Coast basin				
MC-19	granitoid	1,907±0,014	K-Ar biotite (cooling age)	Chalokwu *et al.* (1997)
MC-16B	pegmatite	1,909±0,013	K-Ar muscovite (cooling age)	Chalokwu *et al.* (1997)
MC-16A	pegmatite	1,965±0,013	K-Ar muscovite (cooling age)	Chalokwu *et al.* (1997)
MC-17	pegmatite	2,019±0,014	K-Ar muscovite (cooling age)	Chalokwu *et al.* (1997)
Biriwa	bs	2,072±0,001	U-Pb zircon	Geological map
Besease	bs	2,080±0,003	U-Pb zircon	Geological map
H-CP	granite	2,090±0,001	U-Pb zircon	Davis *et al.* (1994)
Nyan-Komasi	gsb	2,102±0,001	U-Pb zircon	Geological map
Shama	gsb	2,104±0,003	U-Pb zircon	Geological map
GH852	granitoid	2,174±0,002	U-Pb zircon	Oberthür *et al.* (1998)
Daboasi	bmb	2,187±0,001	U-Pb zircon	Geological map
Kisi	bmb	2,187±0,001	U-Pb zircon	Geological map
Ashanti belt				
GH390	basin granitoid	2,097±0,002	Pb-Pb sphene-fsp	Oberthür *et al.* (1998)
GH1017	basin granitoid	2,104±0,002	U-Pb monazite	Oberthür *et al.* (1998)
BPD61	granite	2,159±0,004	U-Pb zircon	Attoh *et al.* (2006)
6427	granitoid	2,172±0,002	U-Pb zircon	Hirdes *et al.* (1992)
Dixcove	gvht	2,172±0,004	U-Pb zircon	Geological map
Kumasi basin				
AK1249	granite	2,090±0,044	U-Pb zircon	Adadey *et al.* (2009)

Table 2. cont.

Sample/Location	Lithology	Age (Ga) ±2σ	Comment	Reference
Kumasi basin cont.				
AK1334	gabbro	2,102±0,013	U-Pb zircon	Adadey *et al.* (2009)
GH388	granitoid	2,105±0,002	Pb-Pb sphene-fsp	Oberthür *et al.* (1998)
GH794	granitoid	2,105±0,003	U-Pb monazite	Oberthür *et al.* (1998)
GH1014	granitoid	2,106±0,002	U-Pb zircon	Oberthür *et al.* (1998)
GH789	granitoid	2,106±0,003	U-Pb monazite	Oberthür *et al.* (1998)
AK4018	granite	2,108±0,018	U-Pb zircon	Adadey *et al.* (2009)
AK5216	granite	2,112±0,019	U-Pb zircon	Adadey *et al.* (2009)
6898A	granitoid	2,116±0,002	U-Pb zircon	Hirdes *et al.* (1992)
AK2091	granodiorite	2,136±0,009	U-Pb zircon	Adadey *et al.* (2009)
AK4124	meta-andesite	2,142±0,024	U-Pb zircon	Adadey *et al.* (2009)
Sefwi belt				
D14	monzonite	2,159±0,004	Pb-Pb zircon	Feybesse *et al.* (2006)
238 - Ivory Coast	monzonite	2,160±0,008	Pb-Pb zircon	Feybesse *et al.* (2006)
227 - Ivory Coast	monzonite	2,161±0,004	Pb-Pb zircon	Feybesse *et al.* (2006)
225 - Ivory Coast	meta-diorite	2,161±0,007	Pb-Pb zircon	Feybesse *et al.* (2006)
6290	granitoid	2,176±0,003	U-Pb zircon in granitoid pebble	Davis *et al.* (1994)
6668	granitoid	2,179±0,002	U-Pb zircon	Hirdes *et al.* (1992)
H285	rhyolite	2,189±0,001	U-Pb zircon	Hirdes & Davis (1998)
G57	gabbro	2,222±0,032	K-Ar Amph	Feybesse *et al.* (2006)
Sunyani basin				
8909A	granitoid	2,088±0,001	U-Pb zircon	Hirdes *et al.* (1992)
-	granite?	2,090±0,001	U-Pb zircon	Zitsmann *et al.* (1997)
Z545	granitoid	2,092±0,002	U-Pb zircon	Zitsmann *et al.* (1997)
-	granite?	2,116±0,002	U-Pb zircon/monazite	Hirdes *et al.* (1993)
Metamorphic ages				
G3 - Suhum	amphibolite lens	1,978±0,037	K-Ar Amph – Contact meta.	Feybesse *et al.* (2006)
G56A - Sefwi	amphibolite in sed.	2,006±0,040	Ar-Ar Amph – Contact meta.	Feybesse *et al.* (2006)
GH794- Kumasi	granitoid	2,086±0,004	Rutile-galena	Oberthür *et al.* (1998)
GH852 - Cape Coast	granitoid	2,092±0,003	U-Pb sphene	Oberthür *et al.* (1998)
G1a1 - Suhum	amphibolite lens	2,095±0,034	K-Ar Hbl	Feybesse *et al.* (2006)
GH789- Kumasi	granitoid	2,098±0,007	Rutile-galena	Oberthür *et al.* (1998)
- Ashanti	dioritic gneiss	<2,100	U-Pb sphene	Loh & Hirdes (1996)

Tidigare skrifter i serien ”Examensarbeten i Geologi vid Lunds Universitet”:

235. Holm, Sanna, 2008: Titanium- and chromium-rich opaque minerals in condensed sediments: chondritic, lunar and terrestrial origins. (30 hskp)
236. Bohlin, Erik & Landen, Ludvig, 2008: Geofysiska mätmetoder för prospektering till ballastmaterial. (30 hskp)
237. Brodén, Olof, 2008: Primär och sekundär migration av hydrokarboner. (15 hskp)
238. Bergman, Bo, 2009: Geofysiska analyser (stångslingram, CVES och IP) av lagerföljd och lakvattenrörelser vid Albäcksdeponin, Trelleborg. (30 hskp)
239. Mehlqvist, Kristina, 2009: The spore record of early land plants from upper Silurian strata in Klinta 1 well, Skåne, Sweden. (45 hskp)
240. Bjärnborg, Karolina, 2009: The copper sulphide mineralization of the Zinkgruvan deposit, Bergslagen, Sweden. (45 hskp)
241. Stenberg, Li, 2009: Historiska kartor som hjälp vid jordartsgeologisk kartering – en pilotstudie från Vångs by i Blekinge. (15 hskp)
242. Nilsson, Mimmi, 2009: Robust U-Pb baddeleyite ages of mafic dykes and intrusions in southern West Greenland: constraints on the coherency of crustal blocks of the North Atlantic Craton. (30 hskp)
243. Hult, Elin, 2009: Oligocene to middle Miocene sediments from ODP leg 159, site 959 offshore Ivory Coast, equatorial West Africa. (15 hskp)
244. Olsson, Håkan, 2009: Climate archives and the Late Ordovician Boda Event. (15 hskp)
245. Wollein Waldetoft, Kristofer, 2009: Svekofennisk granit från olika metamorfa miljöer. (15 hskp)
246. Månsby, Urban, 2009: Late Cretaceous coprolites from the Kristianstad Basin, southern Sweden. (15 hskp)
247. MacGimpsey, I., 2008: Petroleum Geology of the Barents Sea. (15 hskp)
248. Jäckel, O., 2009: Comparison between two sediment X-ray Fluorescence records of the Late Holocene from Disko Bugt, West Greenland; Paleoclimatic and methodological implications. (45 hskp)
249. Andersen, Christine, 2009: The mineral composition of the Burkland Cu-sulphide deposit at Zinkgruvan, Sweden – a supplementary study. (15 hskp)
250. Riebe, My, 2009: Spinel group minerals in carbonaceous and ordinary chondrites. (15 hskp)
251. Nilsson, Filip, 2009: Föroreningsspridning och geologi vid Filborna i Helsingborg. (30 hskp)
252. Peetz, Romina, 2009: A geochemical characterization of the lower part of the Miocene shield-building lavas on Gran Canaria. (45 hskp)
253. Åkesson, Maria, 2010: Mass movements as contamination carriers in surface water systems – Swedish experiences and risks.
254. Löfroth, Elin, 2010: A Greenland ice core perspective on the dating of the Late Bronze Age Santorini eruption. (45 hskp)
255. Ellingsgaard, Óluva, 2009: Formation Evaluation of Interlava Volcaniclastic Rocks from the Faroe Islands and the Faroe-Shetland Basin. (45 hskp)
256. Arvidsson, Kristina, 2010: Geophysical and hydrogeological survey in a part of the Nhandugue River valley, Gorongosa National Park, Mozambique. (45 hskp)
257. Gren, Johan, 2010: Osteo-histology of Mesozoic marine tetrapods – implications for longevity, growth strategies and growth rates. (15 hskp)
258. Syversen, Fredrikke, 2010: Late Jurassic deposits in the Troll field. (15 hskp)
259. Andersson, Pontus, 2010: Hydrogeological investigation for the PEGASUS project, southern Skåne, Sweden. (30 hskp)
260. Noor, Amir, 2010: Upper Ordovician through lowermost Silurian stratigraphy and facies of the Borenshult-1 core, Östergötland, Sweden. (45 hskp)
261. Lewerentz, Alexander, 2010: On the occurrence of baddeleyite in zircon in silica-saturated rocks. (15 hskp)
262. Eriksson, Magnus, 2010: The Ordovician Orthoceratite Limestone and the Blommiga Bladet hardground complex at Horns Udde, Öland. (15 hskp)
263. Lindskog, Anders, 2010: From red to grey and back again: A detailed study of the lower Kundan (Middle Ordovician) ‘Täljsten’ interval and its enclosing strata

in Västergötland, Sweden. (15 hskp)

264. Rääf, Rebecka, 2010: Changes in beyrichiid ostracode faunas during the Late Silurian Lau Event on Gotland, Sweden. (30 hskp)

265. Petersson, Andreas, 2010: Zircon U-Pb, Hf and O isotope constraints on the growth versus recycling of continental crust in the Grenville orogen, Ohio, USA. (45 hskp)

266. Stenberg, Li, 2010: Geophysical and hydrogeological survey in a part of the Nhandugue River valley, Gorongosa National Park, Mozambique – Area 1 and 2. (45 hskp)

267. Andersen, Christine, 2010: Controls of seafloor depth on hydrothermal vent temperatures - prediction, observation & 2D finite element modeling. (45 hskp)

268. März, Nadine, 2010: When did the Kalahari craton form? Constraints from baddeleyite U-Pb geochronology and geo-chemistry of mafic intrusions in the Kaapvaal and Zimbabwe cratons. (45 hskp)

269. Dyck, Brendan, 2010: Metamorphic rocks in a section across a Svecnorwegian eclogite-bearing deformation zone in Halland: characteristics and regional context. (15 hskp)

270. McGimpsey, Ian, 2010: Petrology and lithogeochemistry of the host rocks to the Nautanen Cu-Au deposit, Gällivare area, northern Sweden. (45 hskp)

271. Ulmius, Jan, 2010: Microspherules from the lowermost Ordovician in Scania, Sweden – affinity and taphonomy. (15 hskp)

272. Andersson, Josefin, Hybertsen, Frida, 2010: Geologi i Helsingborgs kommun – en geoturistkarta med beskrivning. (15 hskp)

273. Barth, Kilian, 2011: Late Weichselian glacial and geomorphological reconstruction of South-Western Scania, Sweden. (45 hskp)

274. Mashramah, Yaser, 2011: Maturity of kerogen, petroleum generation and the application of fossils and organic matter for paleotemperature measurements. (45 hskp)

275. Vang, Ina, 2011: Amphibolites, structures and metamorphism on Flekkerøy, south Norway. (45 hskp)

276. Lindvall, Hanna, 2011: A multi-proxy study of a peat sequence on Nightingale Island, South Atlantic. (45 hskp)

277. Bjerg, Benjamin, 2011: Metodik för att förhindra metanemissioner från avfalls-deponier, tillämpad vid Albäcksdeponin, Trelleborg. (30 hskp)

278. Pettersson, Hanna, 2011: El Hicha – en studie av saltstäppssediment. (15 hskp)

279. Dyck, Brendan, 2011: A key fold structure within a Sveconorwegian eclogite-bearing deformation zone in Halland, south-western Sweden: geometry and tectonic implications. (45 hskp)

280. Hansson, Anton, 2011: Torvstratigrafisk studie av en trädstamshorisont i Viss mosse, centrala Skåne kring 4 000 - 3 000 cal BP med avseende på klimat- och vattenståndsförändringar. (15 hskp)

281. Åkesson, Christine, 2011: Vegetations-utvecklingen i nordvästra Europa under Eem och Weichsel, samt en fallstudie av en submorän, organisk avlagring i Bellinga stenbrott, Skåne. (15 hskp)

282. Silveira, Eduardo M., 2011: First precise U-Pb ages of mafic dykes from the São Francisco Craton. (45 hskp)

283. Holm, Johanna, 2011: Geofysisk utvärdering av grundvattenskydd mellan väg 11 och Vombs vattenverk. (15 hskp)

284. Löfgren, Anneli, 2011: Undersökning av geofysiska metoders användbarhet vid kontroll av den omättade zonen i en infiltrationsdamm vid Vombverket. (15 hskp)

285. Grenholm, Mikael, 2011: Petrology of Birimian granitoids in southern Ghana - petrography and petrogenesis. (15 hskp)

LUNDS UNIVERSITET

Geologiska enheten
Institutionen för geo- och ekosystemvetenskaper
Sölvegatan 12, 223 62 Lund